

Projected land ice contributions to twenty-first-century sea level rise

<https://doi.org/10.1038/s41586-021-03302-y>

A list of authors and their affiliations appears at the end of the paper.

Received: 30 December 2019

Accepted: 27 January 2021

Published online: 5 May 2021

 Check for updates

The land ice contribution to global mean sea level rise has not yet been predicted¹ using ice sheet and glacier models for the latest set of socio-economic scenarios, nor using coordinated exploration of uncertainties arising from the various computer models involved. Two recent international projects generated a large suite of projections using multiple models^{2–8}, but primarily used previous-generation scenarios⁹ and climate models¹⁰, and could not fully explore known uncertainties. Here we estimate probability distributions for these projections under the new scenarios^{11,12} using statistical emulation of the ice sheet and glacier models. We find that limiting global warming to 1.5 degrees Celsius would halve the land ice contribution to twenty-first-century sea level rise, relative to current emissions pledges. The median decreases from 25 to 13 centimetres sea level equivalent (SLE) by 2100, with glaciers responsible for half the sea level contribution. The projected Antarctic contribution does not show a clear response to the emissions scenario, owing to uncertainties in the competing processes of increasing ice loss and snowfall accumulation in a warming climate. However, under risk-averse (pessimistic) assumptions, Antarctic ice loss could be five times higher, increasing the median land ice contribution to 42 centimetres SLE under current policies and pledges, with the 95th percentile projection exceeding half a metre even under 1.5 degrees Celsius warming. This would severely limit the possibility of mitigating future coastal flooding. Given this large range (between 13 centimetres SLE using the main projections under 1.5 degrees Celsius warming and 42 centimetres SLE using risk-averse projections under current pledges), adaptation planning for twenty-first-century sea level rise must account for a factor-of-three uncertainty in the land ice contribution until climate policies and the Antarctic response are further constrained.

Land ice has contributed around half of all sea level rise since 1993, and this fraction is expected to increase¹. The Ice Sheet Model Intercomparison Project (ISMIP6)^{2,3} for Coupled Model Intercomparison Project Phase 6 (CMIP6)¹³ and the Glacier Model Intercomparison Project (GlacierMIP)⁴ provide the Intergovernmental Panel on Climate Change (IPCC) with projections of Earth's ice sheet and glacier contributions to future sea level. Both projects use suites of numerical models^{5–8,14,15} and greenhouse gas emission scenarios^{9,11} as the basis of their projections, and various treatments are considered for the interaction between the ice sheets and the ocean^{16–19}. So far, the projects have provided 256 simulations of the Greenland ice sheet, 344 simulations of the Antarctic ice sheet, and 288 simulations of the global glacier response to climate change^{5–8} (see also Extended Data Table 1). Although these simulations and the associated advances^{20,21} represent unprecedented effort, their computational expense and complexity has meant that they (i) focus primarily on previous-generation emissions scenarios (Representation Concentration Pathways⁹, RCPs) developed for the IPCC's Fifth Assessment Report, not the more diverse and policy-relevant Shared Socioeconomic Pathways (SSPs)^{11,22} that underpin the IPCC's Sixth Assessment Report, (ii) are driven mostly by a relatively small number

of older generation global climate models developed before CMIP6¹⁰, and (iii) have incomplete and limited ensemble designs.

To address these limitations, we emulate the future sea level contribution of the 23 regions comprising the world's land ice (see Extended Data Table 2) as a function of global mean surface air-temperature change and as a consequence of marine-terminating glacier retreat in Greenland and ice shelf basal melting and collapse in Antarctica. The ensembles of ice sheet and glacier models are emulated all at once for each region, using their simulations as multiple estimates of sea level contribution for a given set of uncertain input values, and we incorporate the ensemble spread through the use of a 'nugget' term in Gaussian process emulation^{23,24}. Gaussian process regression requires minimal assumptions about the functional form, and provides uncertainty estimates for the emulator predictions²⁵; most previous emulator-type approaches for sea level rise use parametric models, where the functional form is assumed^{26–30}. We then use the emulators to make probabilistic projections for the glacier and ice sheet sea level contributions under five SSPs and under an additional scenario reflecting current climate pledges (nationally determined contributions, NDCs)¹² made under the Paris Agreement. Most projections presented are for the

year 2100, but we also estimate a full timeseries by emulating each year from 2016 to 2100. The details of our emulation approach are described in Methods.

Response to temperature and parameters

Most land ice regions show a fairly linear relationship of increasing mass loss with global mean surface air temperature. Figure 1 shows the temperature dependence of the sea level contribution at 2100 for the ice sheets and peripheral glaciers (Fig. 1a–f) and eleven other glacier regions: four with large maximum contributions (Alaska, Arctic Canada North and South, Russian Arctic; Fig. 1g–j), two with nonlinear temperature dependence, giving near or total disappearance at high temperatures (Central Europe and Caucasus; Fig. 1k, l), and the three regions comprising ‘high mountain’ Asia (Central Asia, South Asia (West) and South Asia (East); Fig. 1m–o), which are important for local water supply³¹. Values of ice sheet parameters are fixed at two possible values for Greenland glacier retreat and Antarctic basal melting, with no Antarctic ice shelf collapse; only simulations using these values are shown. The ensemble designs are not complete—for example, many fewer ice sheet simulations were performed under RCP2.6 than under RCP8.5—so some of the apparent patterns in the simulation data are artefacts of the gaps, which the emulator is intended to account for.

Greenland and the glaciers, which are dominated by surface melting^{5,6,8}, show clear dependence on temperature. Fourteen of the 19 glacier regions show approximately linear relationships, and five are nonlinear (Fig. 1f, k, l; also Western Canada and US, and North Asia, which have weaker nonlinearity: not shown). By contrast, East Antarctica (Fig. 1c) shows a slight decrease in sea level contribution with temperature: snowfall increases, because warmer air can hold more water vapour, and this dominates over the increase in mass loss owing to melting^{7,8}. Finally, West Antarctica and the Peninsula (Fig. 1b, e) show little detectable temperature dependence, owing to an approximate cancellation across varying climate and ice sheet model projections of snowfall accumulation and ice loss. Antarctic ice sheet results are discussed in detail later (see ‘Antarctic focus’).

The ice sheet contributions depend strongly on the Greenland glacier retreat and Antarctic sub-shelf basal melting parameters, which determine the sensitivity of the marine-terminating glaciers to ocean temperatures (and surface meltwater runoff for Greenland). Figure 2 shows these relationships; the Greenland parameter is defined such that more negative values correspond to further retreat inland.

Land ice contributions in 2100

We use probability distributions for global mean surface air temperature (Fig. 3a, Finite amplitude Impulse Response (FaIR) simple climate model)¹² and ice–ocean parameters (Fig. 3b, c shows κ and γ (where κ is the Greenland glacier retreat parameter and γ the Antarctic basal melt parameter), which are derived from the original parameterization studies; ice shelf collapse is assigned equal probability off/on) as inputs to the emulators. Time-series projections for the land ice contribution under all scenarios are shown in Fig. 3d, and probability density functions at 2100 for the Greenland ice sheet, Arctic Canada North, the glacier total, and West and East Antarctica in Fig. 3e–i. The Antarctic ice sheet total under the NDCs is shown in Fig. 3j. (‘Risk-averse’ projections in Fig. 3d, j are discussed later.) Density estimates are less smooth for the glacier and Antarctica totals than individual regions, because sums of regions are estimated by random sampling rather than deterministic integration; these samples are shown for Antarctica (Fig. 3j) and two of the glacier scenarios (Fig. 3g).

Our projections show that reducing greenhouse gas emissions from current and projected pledges under the Paris Agreement (NDCs) enough to limit warming to 1.5 °C (SSP1-19) would nearly

halve the land ice contribution to sea level at 2100 (Table 1: median decreases from 25 cm to 14 cm SLE). This halving is not evenly distributed across the three ice sources: Greenland ice sheet mass losses would reduce by 70%, glacier mass losses by about half, and Antarctica shows little difference between scenarios; this is not due to a lack of change in the Antarctica simulations themselves, but rather to the cancellation of mass gains and losses mentioned above, which varies across models.

Average rates of mass loss for each ice sheet and the glacier total are within 1–2 cm per century of those of the 2013 IPCC Fifth Assessment Report (AR5)²⁶ and the updated assessment for RCP2.6 in the 2019 *IPCC Special Report on the Oceans and Cryosphere in a Changing Climate* (SROCC)¹ (see Methods section ‘Comparison with IPCC assessments’). However, the SROCC revised the projection for Antarctica under RCP8.5 up to 11 cm per century, close to the upper end of our 66% interval for SSP5-85 (though our projections may omit a commitment contribution of up to about 2 cm per century; see Methods). Our results are therefore closer to the 2013 IPCC assessment than to the 2019 assessment with respect to the magnitude and unclear scenario dependence for Antarctica. Our 66% uncertainty intervals are narrower than the IPCC 66% (SROCC) and ≥66% (AR5) uncertainty intervals, as would be expected from the latter being open-ended, except those for Greenland under SSP1-26: too few Greenland simulations were performed under low scenarios (RCP2.6, SSP1-26) to constrain the emulator variance (see Fig. 1a; Methods section ‘Parameter interactions’).

Emulation enables us to additionally assess the sensitivity of projections to uncertainties in their inputs as well as their robustness. If we use CMIP6 global climate models for the projections (Extended Data Fig. 3), instead of FaIR, we find a slight increase in sea level contributions owing to the larger proportion of models with high climate sensitivity to carbon dioxide^{32,33}: the 95th percentile increases by 7 cm under SSP5-85. We estimate the potential impact of reducing uncertainty with future knowledge by using fixed values for temperature, or for the ice sheet retreat and basal melt parameters: the width of the 5–95% ranges reduce by up to 13% and 17% respectively (tests 2–4 in Methods section ‘Sensitivity tests’; Extended Data Table 3, Extended Data Fig. 4). In other words, the ice–ocean interface is a similar magnitude, or larger, contributor to uncertainty in these projections as global warming under a particular emissions scenario. When we assess the robustness of the projections to different selections and treatments of the ice sheet simulations, we find this makes very little difference (tests 2–4 in Methods section ‘Robustness checks’; Extended Data Table 4, Extended Data Fig. 5).

Antarctic focus

No clear dependence on emissions scenario emerges for Antarctica. This is partly due to the opposite scenario dependencies of the West and East Antarctica regions (Fig. 3f, g). But the average response to emissions scenario for each region is also small. A key reason is the wide variety of changes in the atmosphere and ocean in the global climate models. Figure 4 shows ice sheet model simulations where both the high- and low-emissions scenario were run (two climate models for Greenland, three for Antarctica). For the Greenland ice sheet, all simulations predict increased mass loss under higher emissions (Fig. 4a, red shaded region). For Antarctica, the picture is more complex, and mostly clustered according to the climate model. Many West Antarctica simulations show the same straightforward response as Greenland (Fig. 4b), particularly those that do not use the ISMIP6 basal melting parameterization (see Methods). However, the West Antarctica simulations driven by CNRM-CM6-1 show the reverse, where mass gain through snowfall accumulation increases more under high emissions than mass loss (which is predominantly ocean-induced). (Note that fewer simulations were driven by IPSL-CM5A-MR and CNRM-CM6-1 than by NorESM1-M, so their spread is necessarily smaller). East Antarctica

Article

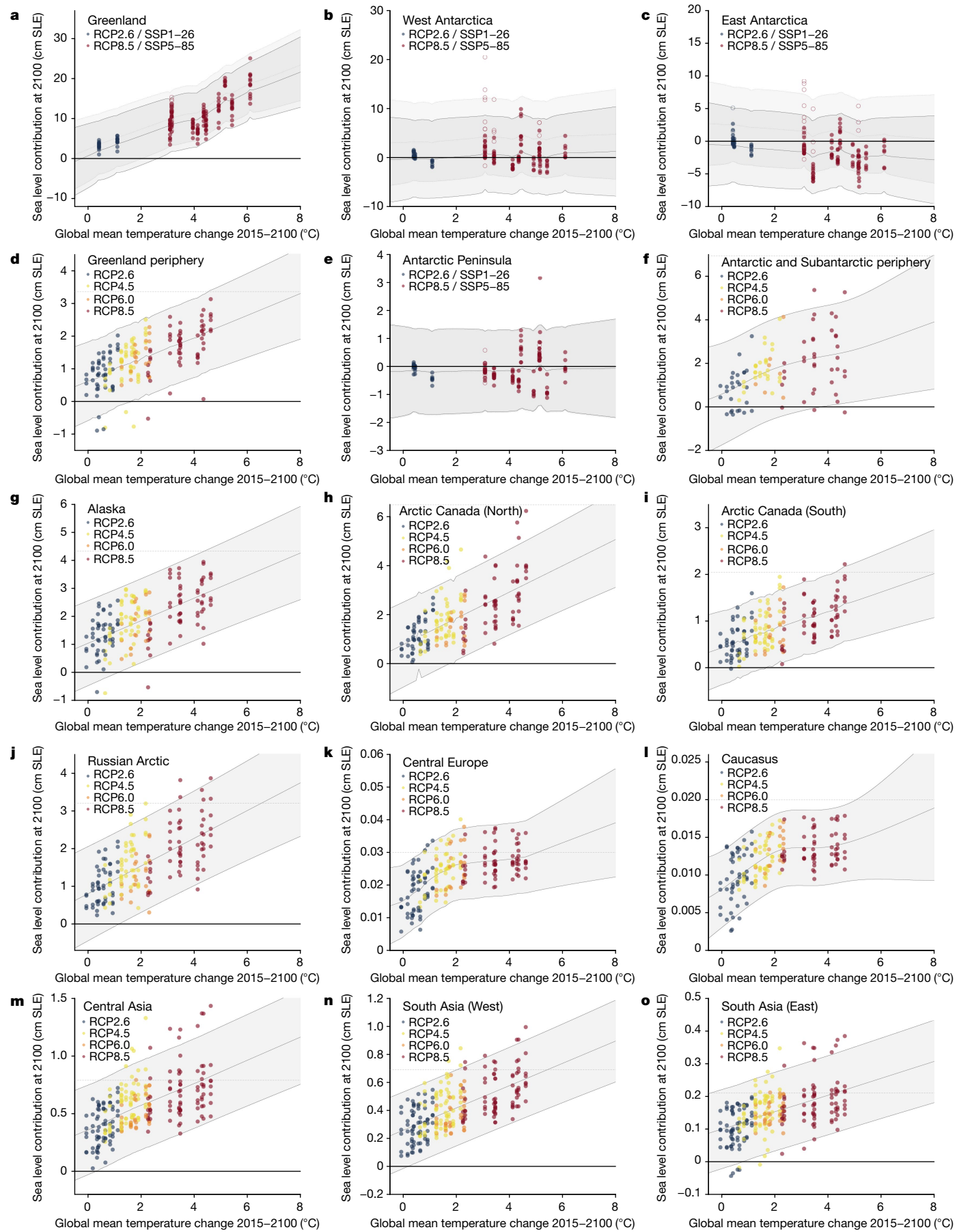


Fig. 1 | See next page for caption.

Fig. 1 | Ice sheet and glacier mass loss generally increases linearly with global mean temperature. **a–o**, Projected mass changes from 2015–2100 in sea level equivalent (SLE) as a function of global mean surface air temperature change over the same period for Greenland ice sheet (**a**); West and East Antarctic ice sheets (**b**, **c**); Greenland peripheral glaciers (**d**); the Antarctic Peninsula and Antarctic peripheral glaciers (**e**, **f**); four glacier regions with large maximum sea level contributions (Alaska, Arctic Canada North and South, Russian Arctic; **g–j**); two regions with nonlinear temperature dependence and total or near-total disappearance projected at high temperatures (Central Europe and Caucasus; **k**, **l**); and three regions comprising high mountain Asia (**m–o**). Central solid lines show the emulator mean, and shaded regions the mean ± 2 s.d. For the ice sheets (**a–c**, **e**), darker shaded regions use parameter

values fixed at their default values (Greenland glacier retreat: median; Antarctic sub-shelf basal melting: median of Mean Antarctic distribution; Antarctic ice shelf collapse off), and lighter shaded regions use alternative values (Greenland: 75th percentile; Antarctica: median of Pine Island Glacier distribution). See Methods for details. Points show ice sheet and glacier simulations under RCP2.6/SSP1-26 (blue), RCP4.5 (yellow), RCP6.0 (orange) and RCP8.5/SSP5-85 (red). Solid circles for the ice sheets use the default ice–ocean parameter value and open circles use the alternative value (other simulations are not shown). Glacier simulations are change in total volume, not volume above flotation; the estimated maximum sea level contribution (that is, current total glacier volume above flotation)⁴⁴ is shown (horizontal dashed line).

and the Antarctic Peninsula mostly show this latter response, though some simulations show other combinations: more mass loss under low emissions than high, or mass loss under low emissions and mass gain under high.

It is challenging to evaluate which of these three climate models, or others used by ISMIP6, are most reliable for Antarctic climate change. Ocean conditions and accumulation show large spatio-temporal variability and are sparsely observed; models imperfectly represent important processes, and it is unclear whether the newer CMIP6 models have improved relative to CMIP5^{19,34–37}. Most of the climate models were from CMIP5, including NorESM1-M and IPSL-CM5A-MR, and were selected by their success at reproducing southern climatological observations (while also sampling a range of future climate responses)²¹. NorESM1-M

has a lower-than-average atmospheric warming, hence less snowfall, whereas IPSL-CM5A-MR has a higher-than-average atmospheric warming (particularly for East Antarctica)²¹. The newer CMIP6 models, including CNRM-CM6-1, were selected only by their availability. Changing the selection or treatment of Antarctica simulations—for example, using subsets of climate models, or rejecting simulations with net mass gain early in the projections—do not result in any substantial scenario dependence (see tests 7–10 in Methods section ‘Robustness checks’; Extended Data Table 4, Extended Data Fig. 5).

Uncertainty about the scenario dependence of Antarctic projections is not new. The IPCC Fifth Assessment Report (2013) stated “the current state of knowledge does not permit a quantitative assessment”²⁶ of the dependence of rapid dynamical change on scenario. Some studies that

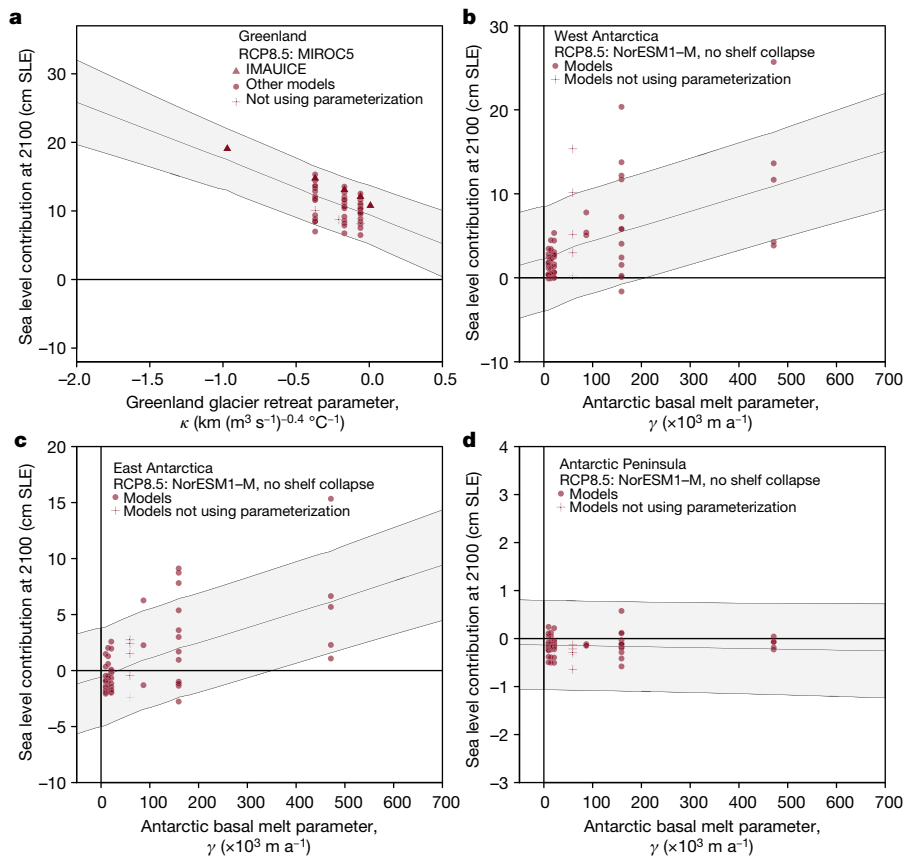


Fig. 2 | Ice sheet mass loss strongly depends on ice–ocean parameters. **a–d**, Projections of sea level contribution from 2015–2100 as a function of Greenland glacier retreat parameter (κ ; **a**), and Antarctic basal melt parameter (γ ; metres per year, m a^{-1}) for West Antarctica (**b**), East Antarctica (**c**), Peninsula (**d**). Solid line shows emulator mean estimate using fixed global temperature (projected by the global climate model most used for simulations, under RCP8.5), and shaded regions show the mean ± 2 s.d. Symbols show ice sheet models forced by this climate model for which simulations for at least three (Greenland) or four (Antarctic) melt parameter values were available: circles use the ISMIP6 parameterization for the ice–ocean interface; crosses use other representations, and are assigned ensemble mean values of the parameter; triangles show the Greenland ice sheet model for which two additional values of κ were run.

and shaded regions show the mean ± 2 s.d. Symbols show ice sheet models forced by this climate model for which simulations for at least three (Greenland) or four (Antarctic) melt parameter values were available: circles use the ISMIP6 parameterization for the ice–ocean interface; crosses use other representations, and are assigned ensemble mean values of the parameter; triangles show the Greenland ice sheet model for which two additional values of κ were run.

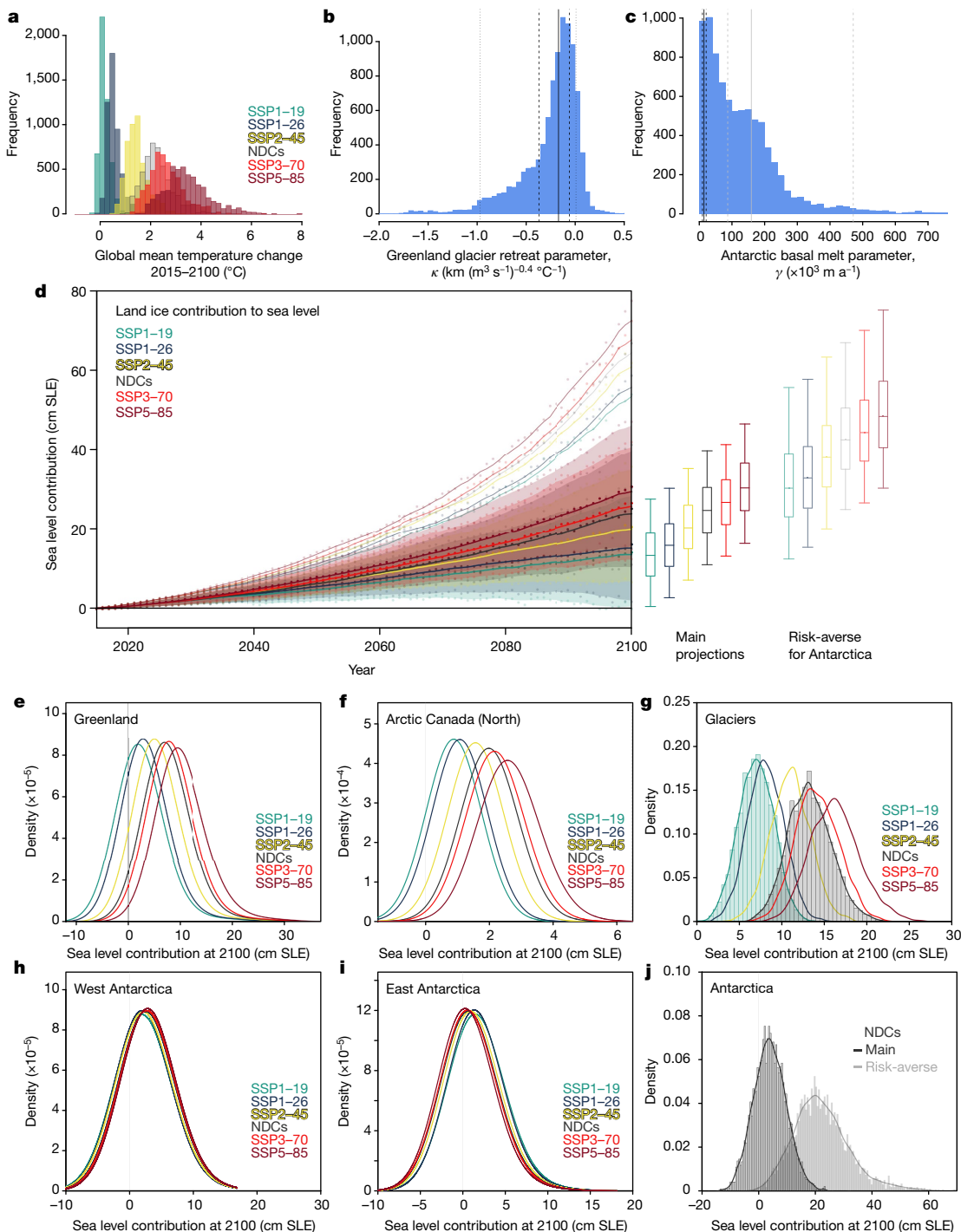


Fig. 3 | Projected land ice contribution to 21st-century sea level rise and for selected regions at 2100. **a**, Probability distributions for global mean surface air temperature change from 2015–2100 from the Fair simple climate model under the five SSPs and current NDCs ($N=5,000$ each). **b**, Greenland ice sheet retreat parameter (κ) distribution ($N=10,000$); vertical lines show the five values used for simulations: median (solid), 25th and 75th percentiles (dashed), and 5th and 95th percentiles (dotted). **c**, Antarctic basal melt parameter (γ) distribution ($N=8,200$); vertical lines show the six values used for simulations: median (solid), 5th and 95th percentiles (dashed) of the Mean Antarctic (black) and Pine Island Glacier (grey) distributions (see Methods). **d**, Projected land ice contribution to sea level (in cm SLE) from 2015–2100 under the five SSPs and NDCs. Solid lines and shaded regions: median and 5th–95th percentiles ($N=11,500$ per year per scenario); five-year smoothing applied, with original data shown as dots (interannual variation arises from annual sampling of

emulator uncertainties). Pale solid lines: 95th percentiles of risk-averse projections. Box and whiskers show [5, 25, 50, 75, 95]th percentiles at 2100 ($N=115,000$ per scenario) for main projections (left) and risk-averse projections for Antarctica (right). **e–j**, Probability density functions for 2100 estimated for: Greenland ice sheet (**e**), Arctic Canada North (**f**), total for glaciers (**g**), West and East Antarctica (**h**, **i**) for all scenarios, and total for Antarctic ice sheet under main and risk-averse projections for the NDCs (**j**). Glacier and Antarctic totals are less smooth because they are estimated from a sum of Monte Carlo samples from each region, rather than deterministic integration (see Methods); these samples are shown for SSP1-19 and NDCs ($N=5,000$). Ice sheet projections do not include the response to pre-2015 climate forcing, which is estimated to add less than 1 cm to the Greenland contribution and up to -2 cm to the Antarctic (see Methods).

Table 1 | Projected land ice contributions to sea level rise in 2100 under different greenhouse gas scenarios and Antarctic modelling assumptions

	Main projections		Risk-averse projections	
	50th [5th, 95th] percentiles (cm SLE)	[17th, 83rd] percentiles (cm SLE)	50th [5th, 95th] percentiles (cm SLE)	[17th, 83rd] percentiles (cm SLE)
Global glaciers				
SSP1-19	7 [4, 10]	[5, 9]		
SSP1-26	8 [5, 12]	[6, 10]		
SSP2-45	11 [7, 15]	[9, 13]		
NDCs	13 [9, 18]	[11, 16]		
SSP3-70	14 [10, 19]	[12, 17]		
SSP5-85	16 [12, 21]	[14, 19]		
Greenland ice sheet				
SSP1-19	2 [-6, 11]	[-2, 7]		
SSP1-26	3 [-4, 12]	[-1, 8]		
SSP2-45	5 [-2, 14]	[1, 10]		
NDCs	7 [0, 16]	[3, 12]		
SSP3-70	8 [0, 17]	[4, 13]		
SSP5-85	10 [2, 20]	[5, 15]		
Antarctic ice sheet				
SSP1-19	4 [-5, 14]	[-1, 10]	21 [6, 42]	[12, 32]
SSP1-26	4 [-5, 14]	[-1, 10]	21 [7, 43]	[12, 31]
SSP2-45	4 [-5, 14]	[-1, 9]	21 [7, 43]	[12, 31]
NDCs	4 [-5, 14]	[-1, 10]	21 [7, 43]	[13, 31]
SSP3-70	4 [-5, 14]	[-1, 10]	21 [8, 43]	[13, 31]
SSP5-85	4 [-5, 14]	[-1, 10]	22 [8, 43]	[14, 32]
Land ice				
SSP1-19	13 [0, 28]	[6, 21]	30 [12, 56]	[20, 43]
SSP1-26	16 [3, 30]	[8, 24]	33 [15, 58]	[22, 45]
SSP2-45	20 [7, 35]	[13, 28]	38 [20, 63]	[28, 50]
NDCs	25 [11, 40]	[17, 33]	42 [25, 67]	[32, 54]
SSP3-70	27 [13, 41]	[19, 35]	44 [27, 70]	[34, 56]
SSP5-85	30 [16, 46]	[22, 39]	48 [30, 75]	[38, 61]

Projected changes to global glaciers, Greenland and Antarctic ice sheets and land ice total from 2015–2100 in sea level equivalent (cm SLE) for five SSPs and predicted emissions under the 2019 NDCs. Ice sheet projections do not include the response to pre-2015 climate forcing, which is estimated to add less than 1 cm to the Greenland contribution and approximately 2 cm to the Antarctic (see Methods). The glaciers include the Greenland and Antarctic peripheral glaciers; the overlap of Antarctic periphery glaciers with the ice sheet contribution is estimated to be less than 1 cm SLE.

show strong scenario dependence neglect the compensating accumulation part^{27,38}, use extreme¹ ice shelf collapse scenarios^{25,41}, or the basal melt parameterization uncertainty is the same order of magnitude as, or larger than, the scenario dependence^{28,39,40}. To be clear, we do not assert that Antarctica's future does not depend on future greenhouse emissions or global warming; only that the relationship between global and Antarctic climate change, and the ice sheet's response, are complex, only partially understood, and involve compensating factors of increasing mass loss and gain that result in a balance we are not yet confident about.

We test the sensitivity of the Antarctica projections to the basal melting parameter. The main projections combine two distributions¹⁹ for γ derived from observations of mean Antarctic basal melt rates or the ten highest melt rates for Pine Island Glacier (see Methods). Using only the mean distribution decreases the median to approximately 0 cm SLE and the 95th percentile to approximately 8 cm SLE for all scenarios;

using only the high distribution has less effect, increasing the median to 6 cm SLE and the 95th percentile to approximately 16 cm SLE (Extended Data Table 3, Extended Data Fig. 4: tests 5, 6). We also try and reproduce the higher projections of ref.²⁷ using a similar approach to sampling basal melt (see Methods), and find we only obtain similar projections when using extreme values of our parameter range (Extended Data Table 3, Extended Data Fig. 4: tests 7, 8). This suggests that ref.²⁷ could be interpreted as more pessimistic projections: they use values of basal melt sensitivity to ocean temperature consistent with those estimated for the Amundsen Sea region³⁸, which is currently undergoing most change.

However, other factors can lead to similarly high projections. In particular, the sensitivity of an individual ice sheet model to the basal melt parameter can have a large effect. This differs widely across ice sheet models, and the net contribution also depends on the climate model (Extended Data Fig. 6). Emulator projections based on a single model with high or low sensitivity are shown in Extended Data Fig. 5 (tests 4, 5; Extended Data Table 4). These also do not show strong scenario dependence—just a 2–3-cm decrease under high emissions for the low sensitivity model, because the snowfall effect is more apparent—but instead predict a high or low sea level contribution, respectively, regardless of scenario (95th percentiles: 29–30 cm and 7–9 cm). The high sensitivity of the first model (SICOPOLIS) is probably due to the way that sub-shelf melting is applied: over entire grid cells along the grounding line, rather than just the parts detected as floating²⁷. We also show results from the four most sensitive models, which are similarly high (Extended Data Table 4, Extended Data Fig. 5: test 6). We do not have sufficient observations to evaluate which ice sheet models have the most realistic response, nor sufficient understanding to confidently predict how basal melt sensitivity might change in future^{19,35}, and therefore use all models in the main projections (see also 'Risk-averse projections', below).

The ice shelf collapse scenario has little effect on our projections. Switching it on increases the Antarctic Peninsula and East Antarctic median contributions by 1 cm and 0–1 cm SLE from 2015–2100, with no change for West Antarctica (Extended Data Table 3, Extended Data Fig. 4: tests 9, 10). This is similar, within uncertainties, to the ice sheet simulations (Extended Data Fig. 7). The effect is small because surface meltwater is not projected to be enough to cause collapses until the second half of the century, and even then only for small number of shelves, mostly around the Peninsula⁷. Some combinations of climate and ice sheet models do project larger sea level contributions—in particular, 5 cm for East Antarctica from the SICOPOLIS ice sheet model driven by HadGEM2-ES. The HadGEM2-ES climate model projects extreme ocean warming in the Ross Sea²¹, while SICOPOLIS has one of the largest responses among the ice sheet models (as described above). If these two were found to be the most realistic models, then the ISMIP6 ensemble and emulator may underestimate the effect of ice shelf collapse by a few centimetres. Further results are in Methods section 'Parameter interactions'.

Risk-averse projections

Given the wide range and cancellations of responses across models and parameters, we present alternative Antarctic projections we judge to be pessimistic but physically plausible for the use of risk-averse stakeholders, by combining a set of assumptions that lead to high sea level contributions. These are: the four ice sheet models most sensitive to basal melting; the four climate models that lead to highest Antarctic sea level contributions, and the one used to drive most of the ice shelf collapse simulations; the high basal melt (Pine Island Glacier) distribution; and with ice shelf collapse 'on' (that is, combining robustness tests 6, 7 and sensitivity tests 6, 10). This storyline would come about if the high basal melt sensitivities currently observed at Pine Island Glacier soon become widespread around the continent; the ice sheet responds to

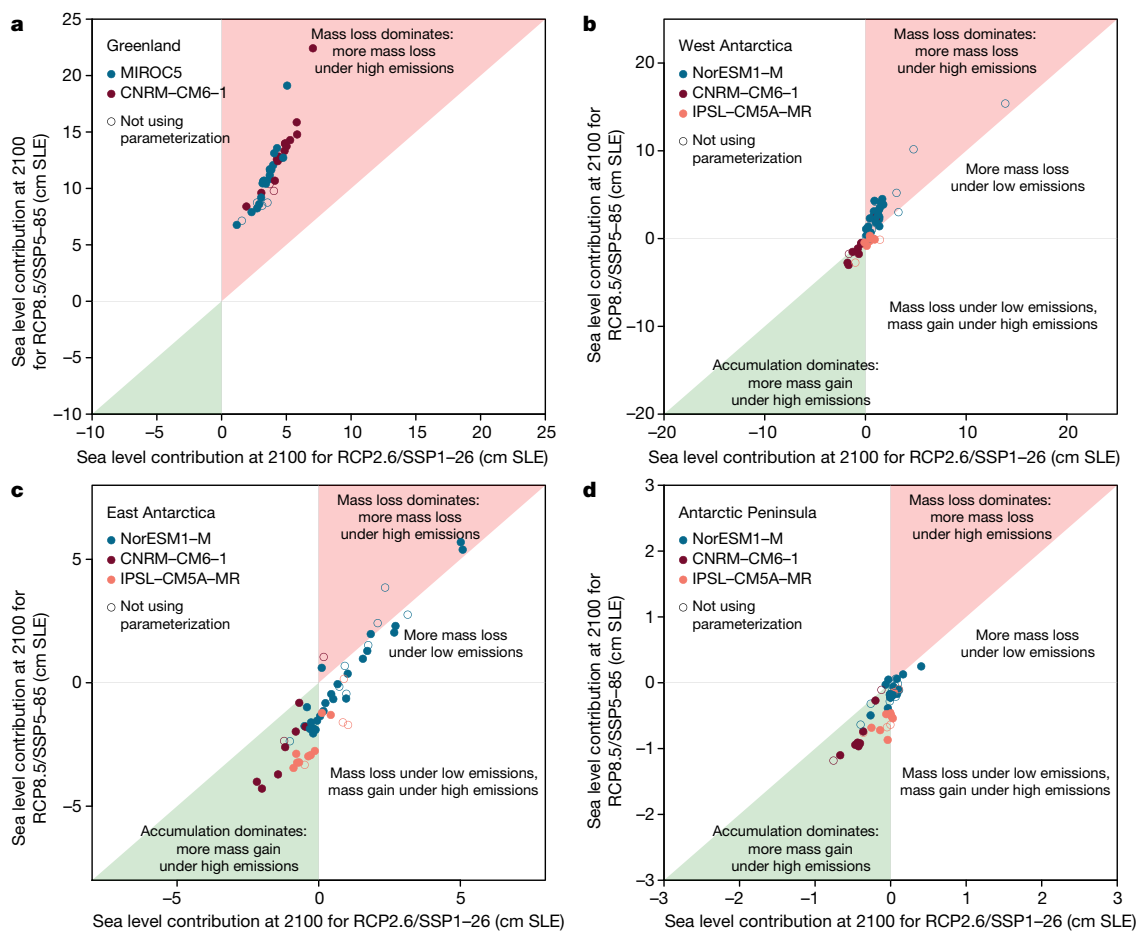


Fig. 4 | Climate and ice sheet projections show a wide range of responses to greenhouse gas emissions scenario. Sea level contribution at 2100 under high greenhouse gas emissions scenarios (RCP8.5 or SSP5-85) versus low scenarios (RCP2.6 or SSP1-26), categorized by climate model forcing (NorESM1-M and IPSL-CM5A-MR use RCPs; CNRM-CM6-1 use SSPs), without ice shelf collapse. **a**, Greenland. **b**, West Antarctica. **c**, East Antarctica. **d**, Antarctic Peninsula.

Filled circles show ice sheet models that use the ISMIP6 parameterizations of the ice–ocean interface, and open circles show models that use their own. Simulations in the red shaded regions have more mass loss under high emissions (RCP8.5/SSP5-85) than low (RCP1-26/SSP1-26); those in the green shaded regions have more mass gain under high emissions scenarios than low. Two regions with other possible combinations are also labelled.

these with extensive retreat and rapid ice flow, and atmospheric warming is sufficient to disintegrate ice shelves, but does not substantially increase snowfall. The risk-averse projections are more than five times the main estimates: median 21 cm (5–95% range 7 to 43 cm) under the NDCs (Fig. 3j), and essentially the same under SSP5-85 (Table 1; regions shown in Extended Data Fig. 4, test 11), with the 95th percentiles emerging above the main projections after 2040 (Fig. 3d). This is very similar to projections²⁵ under an extreme scenario of widespread ice shelf collapses for RCP8.5 (median 21 cm; 5–95% range 9 to 39 cm). The median is higher than ref.²⁷ for RCP8.5, though the 95th percentile is smaller. No models that include a representation of rapid ice cliff collapse through the proposed ‘Marine Ice Cliff Instability’⁴¹ mechanism participated in ISMIP6. This hypothesis is the process with the largest estimated systematic impact on projections: it could increase projections by tens of centimetres if both the mechanism and projections of extreme ice shelf collapse are found to be robust^{25,42}.

Our risk-averse Antarctica projections increase the total land ice sea level contribution to 42 cm (5–95% range 25 to 67 cm) SLE under current policies and pledges (NDCs), and to 30 cm (5–95% range 12 to 56 cm) SLE even under SSP1-19. This means that plausible modelling choices for Antarctica could change the median land ice contribution by more (17 cm SLE) than the difference between these emissions scenarios (12 cm SLE). This ambiguity limits confidence in assessing the effectiveness of mitigation on the response of global land ice to climate change. When combined, the effects of uncertain emissions and

Antarctic response lead to a threefold spread in median projections of the land ice contribution to sea level rise, ranging from 13 to 42 cm SLE over 2015–2100, implying that flexible adaptation under substantial uncertainty will be essential until either can be further constrained.

Not all modelling uncertainties could be systematically assessed here. Aside from the ice-cliff instability hypothesis, these include ice sheet basal hydrology and sliding; glacier model parameters, ice–water interactions and meltwater routeing; model initialization; and the use of coarse-resolution global climate models (and a single high-resolution regional climate model for the Greenland ice sheet). The probabilities we present are therefore specific to our ensembles, and adding new climate and ice sheet models, or exploration of new parameters, could shift or broaden their distributions⁴³. However, our projections demonstrate the importance of systematic design to assess as many uncertainties as feasible, and represent the current state-of-the-art in estimating the land ice contribution to global mean sea level rise.

Online content

Any methods, additional references, Nature Research reporting summaries, source data, extended data, supplementary information, acknowledgements, peer review information; details of author contributions and competing interests; and statements of data and code availability are available at <https://doi.org/10.1038/s41586-021-03302-y>.

- Oppenheimer, M. et al. Sea Level Rise and Implications for Low-Lying Islands, Coasts and Communities. In *IPCC Special Report on the Ocean and Cryosphere in a Changing Climate* (eds Pörtner, H.-O. et al.) (IPCC, 2019).
 - Nowicki, S. M. J. et al. Ice Sheet Model Intercomparison Project (ISMIP6) contribution to CMIP6. *Geosci. Model Dev.* **9**, 4521–4545 (2016).
 - Nowicki, S. et al. Experimental protocol for sea level projections from ISMIP6 stand-alone ice sheet models. *Cryosphere* **14**, 2331–2368 (2020).
 - Hock, R. et al. GlacierMIP – a model intercomparison of global-scale glacier mass-balance models and projections. *J. Glaciol.* **65**, 453–467 (2019).
 - Marzeion, B. et al. Partitioning the uncertainty of ensemble projections of global glacier mass change. *Earth's Future* **8**, e2019EF001470 (2020).
 - Goelzer, H. et al. The future sea-level contribution of the Greenland ice sheet: a multi-model ensemble study of ISMIP6. *Cryosphere* **14**, 3071–3096 (2020).
 - Seroussi, H. et al. ISMIP6 Antarctica: a multi-model ensemble of the Antarctic ice sheet evolution over the 21st century. *Cryosphere* **14**, 3033–3070 (2020).
 - Payne, A. et al. Future sea level change under CMIP5 and CMIP6 scenarios from the Greenland and Antarctic ice sheets. *Geophys. Res. Lett.* (in the press).
 - van Vuuren, D. P. et al. The representative concentration pathways: an overview. *Clim. Change* **109**, 5–31 (2011).
 - Taylor, K. E., Stouffer, R. J. & Meehl, G. A. An overview of CMIP5 and the experiment design. *Bull. Am. Meteorol. Soc.* **93**, 485–498 (2012).
 - Riahi, K. et al. The Shared Socioeconomic Pathways and their energy, land use, and greenhouse gas emissions implications: an overview. *Glob. Environ. Change* **42**, 153–168 (2017).
 - McKenna, C. M. et al. Stringent mitigation substantially reduces risk of unprecedented near-term warming rates. *Nat. Clim. Change* **11**, 126–131 (2021).
 - Eyring, V. et al. Overview of the Coupled Model Intercomparison Project Phase 6 (CMIP6) experimental design and organization. *Geosci. Model Dev.* **9**, 1937–1958 (2016).
 - Goelzer, H. et al. Design and results of the ice sheet model initialisation experiments initMIP-Greenland: an ISMIP6 intercomparison. *Cryosphere* **12**, 1433–1460 (2018).
 - Seroussi, H. et al. initMIP-Antarctica: an ice sheet model initialization experiment of ISMIP6. *Cryosphere* **13**, 1441–1471 (2019).
 - Slater, D. A. et al. Estimating Greenland tidewater glacier retreat driven by submarine melting. *Cryosphere* **13**, 2489–2509 (2019).
 - Slater, D. A. et al. Twenty-first-century ocean forcing of the Greenland ice sheet for modelling of sea level contribution. *Cryosphere* **14**, 985–1008 (2020).
 - Favier, L. et al. Assessment of sub-shelf melting parameterisations using the ocean-ice-sheet coupled model NEMO(v3.6)-Elmer/Ice(v8.3). *Geosci. Model Dev.* **12**, 2255–2283 (2019).
 - Jourdain, N. C. et al. A protocol for calculating basal melt rates in the ISMIP6 Antarctic ice sheet projections. *Cryosphere* **14**, 3111–3134 (2020).
 - Goelzer, H. et al. Remapping of Greenland ice sheet surface mass balance anomalies for large ensemble sea-level change projections. *Cryosphere* **14**, 1747–1762 (2020).
 - Barthel, A. et al. CMIP5 model selection for ISMIP6 ice sheet model forcing: Greenland and Antarctica. *Cryosphere* **14**, 855–879 (2020).
 - O'Neill, B. C. et al. The Scenario Model Intercomparison Project (ScenarioMIP) for CMIP6. *Geosci. Model Dev.* **9**, 3461–3482 (2016).
 - Andrianakis, I. & Challenor, P. G. The effect of the nugget on Gaussian process emulators of computer models. *Comput. Stat. Data Anal.* **56**, 4215–4228 (2012).
 - Gramacy, R. B. & Lee, H. K. H. Cases for the nugget in modeling computer experiments. *Stat. Comput.* **22**, 713–722 (2012).
 - Edwards, T. L. et al. Revisiting Antarctic ice loss due to marine ice cliff instability. *Nature* **566**, 58–64 (2019).
 - Church, J. A. et al. Sea level change. In *Climate Change 2013: The Physical Science Basis. Contribution of Working Group I to the Fifth Assessment Report of the Intergovernmental Panel on Climate Change* (eds Stocker, T. F. et al.) Ch. 13 (Cambridge Univ. Press, 2013).
 - Levermann, A. et al. Projecting Antarctica's contribution to future sea level rise from basal ice shelf melt using linear response functions of 16 ice sheet models (LARMIP-2). *Earth Syst. Dynam.* **11**, 35–76 (2020).
 - Bulthuis, K. et al. Uncertainty quantification of the multi-centennial response of the Antarctic ice sheet to climate change. *Cryosphere* **13**, 1349–1380 (2019).
 - Naueis, A. et al. Synthesizing long-term sea level rise projections – the MAGICC sea level model v2.0. *Geosci. Model Dev.* **10**, 2495–2524 (2017).
 - Palmer, M. D. et al. Exploring the drivers of global and local sea-level change over the 21st century and beyond. *Earth's Future* **8**, e2019EF001413 (2020).
 - Biemanns, H. et al. Importance of snow and glacier meltwater for agriculture on the Indo-Gangetic Plain. *Nature Sustain.* **2**, 594–601 (2019).
 - Forster, P. M., Maycock, A. C., McKenna, C. M. & Smith, C. J. Latest climate models confirm need for urgent mitigation. *Nat. Clim. Change* **10**, 7–10 (2019).
 - Meehl, G. et al. Context for interpreting equilibrium climate sensitivity and transient climate response from the CMIP6 Earth system models. *Sci. Adv.* **6**, eaaba1981 (2020).
 - Meredith, M. et al. Polar Regions. In *IPCC Special Report on the Ocean and Cryosphere in a Changing Climate* (eds Pörtner, H.-O. et al.) Ch. 3 (2019).
 - Naughten, K. A. et al. Future projections of Antarctic ice shelf melting based on CMIP5 scenarios. *J. Clim.* **31**, 5243–5261 (2018).
 - Mottram, R. et al. What is the surface mass balance of Antarctica? An intercomparison of regional climate model estimates. Preprint at <https://doi.org/10.5194/tc-2019-333> (2020).
 - Roussel, M.-L., Lemonnier, F., Genthon, C. & Krinner, G. Evaluating Antarctic precipitation in ERA5 and CMIP6 against CloudSat observations. *Cryosphere* **14**, 2715–2727 (2020).
 - Reese, R. et al. The role of history and strength of the oceanic forcing in sea level projections from Antarctica with the Parallel Ice Sheet Model. *Cryosphere* **14**, 3097–3110 (2020).
 - Golledge, N. R. et al. The multi-millennial Antarctic commitment to future sea-level rise. *Nature* **526**, 421–425 (2015).
 - Golledge, N. R. et al. Global environmental consequences of twenty-first-century ice-sheet melt. *Nature* **566**, 65–72 (2019).
 - DeConto, R. M. & Pollard, D. Contribution of Antarctica to past and future sea-level rise. *Nature* **531**, 591–597 (2016).
 - Clerc, F., Minchew, B. M. & Behn, M. D. Marine ice cliff instability mitigated by slow removal of ice shelves. *Geophys. Res. Lett.* **46**, 12108–12116 (2019).
 - Williamson, D. B. & Sansom, P. G. How are emergent constraints quantifying uncertainty and what do they leave behind? *Bull. Am. Meteorol. Soc.* **100**, 2571–2588 (2019).
 - Farinotti, D. et al. A consensus estimate for the ice thickness distribution of all glaciers on Earth. *Nat. Geosci.* **12**, 168–173 (2019).
- Publisher's note** Springer Nature remains neutral with regard to jurisdictional claims in published maps and institutional affiliations.
- © The Author(s), under exclusive licence to Springer Nature Limited 2021

Tamsin L. Edwards¹ , Sophie Nowicki^{2,3}, Ben Marzeion^{4,5}, Regine Hock^{6,7}, Heiko Goelzer^{8,9,10}, Hélène Seroussi¹¹, Nicolas C. Jourdain¹², Donald A. Slater^{13,14,15}, Fiona E. Turner¹, Christopher J. Smith^{16,17}, Christine M. McKenna¹⁶, Erika Simon², Ayako Abe-Ouchi¹⁸, Jonathan M. Gregory^{19,20}, Eric Larour¹¹, William H. Lipscomb²¹, Antony J. Payne²², Andrew Shepherd²³, Cécile Agosta²⁴, Patrick Alexander^{25,26}, Torsten Albrecht²⁷, Brian Anderson²⁸, Xylar Asay-Davis²⁹, Andy Aschwanden⁶, Alice Barthel²⁹, Andrew Bliss³⁰, Reinhard Calov²⁷, Christopher Chambers³¹, Nicolas Champollion^{4,12}, Youngmin Choi^{11,32}, Richard Cullather², Joshua Cuzzone¹¹, Christophe Dumas²⁴, Denis Felikson^{2,33}, Xavier Fettweis³⁴, Koji Fujita³⁵, Benjamin K. Galton-Fenzi^{36,37}, Rupert Gladstone³⁸, Nicholas R. Golledge²⁸, Ralf Greve^{31,39}, Tore Hattermann^{40,41}, Matthew J. Hoffman²⁹, Angelika Humbert^{42,44}, Matthias Huss^{44,45,46}, Philippe Huybrechts⁴⁷, Walter Immerzeel⁴⁸, Thomas Kleiner⁴², Philip Kraaijenbrink⁴⁸, Sébastien Le clec'h⁴⁷, Victoria Lee⁴⁹, Gunter R. Leguy²¹, Christopher M. Little⁵⁰, Daniel P. Lowry⁵¹, Jan-Hendrik Malles⁴⁵, Daniel F. Martin⁵², Fabien Maussion⁵³, Mathieu Morlighem³², James F. O'Neill¹, Isabel Nias^{2,54}, Frank Pattyn⁹, Tyler Pelle³², Stephen F. Price²⁹, Aurélien Quiquet²⁴, Valentina Radic⁵⁵, Ronja Reese²⁷, David R. Rounce^{6,56}, Martin Rückamp⁴², Akiko Sakai³⁵, Courtney Shafer⁵², Nicole-Jeanne Schlegel¹¹, Sarah Shannon²², Robin S. Smith¹⁹, Fiammetta Straneo¹³, Sainan Sun⁹, Lev Tarasov⁵⁷, Luke D. Trusel⁵⁸, Jonas Van Breedam⁴⁷, Roderik van de Wal^{48,49}, Michiel van den Broeke⁸, Ricarda Winkelmann^{27,59}, Harry Zekollari^{9,44,45,60}, Chen Zhao³⁷, Tong Zhang^{29,61} & Thomas Zwinger⁶²

¹Department of Geography, King's College London, London, UK. ²NASA Goddard Space Flight Center, Greenbelt, MD, USA. ³Geology Department and RENEW Institute, University at Buffalo, Buffalo, NY, USA. ⁴Institute of Geography, University of Bremen, Bremen, Germany. ⁵MARUM – Center for Marine Environmental Sciences, University of Bremen, Bremen, Germany. ⁶Geophysical Institute, University of Alaska Fairbanks, Fairbanks, USA. ⁷Department of Geosciences, University of Oslo, Oslo, Norway. ⁸Institute for Marine and Atmospheric Research Utrecht, Utrecht University, Utrecht, The Netherlands. ⁹Laboratoire de Glaciologie, Université Libre de Bruxelles, Brussels, Belgium. ¹⁰NORCE Norwegian Research Centre, Bjerknes Centre for Climate Research, Bergen, Norway. ¹¹Jet Propulsion Laboratory, California Institute of Technology, Pasadena, CA, USA. ¹²Institut des géosciences de l'environnement, Université Grenoble Alpes, CNRS, IRD, G-INP, Grenoble, France. ¹³Scripps Institution of Oceanography, University of California San Diego, La Jolla, CA, USA. ¹⁴School of Geography and Sustainable Development, University of St Andrews, St Andrews, UK. ¹⁵School of Geosciences, University of Edinburgh, Edinburgh, UK. ¹⁶Priestley International Centre for Climate, University of Leeds, Leeds, UK. ¹⁷International Institute for Applied Systems Analysis (IIASA), Laxenburg, Austria. ¹⁸Atmosphere and Ocean Research Institute, The University of Tokyo, Tokyo, Japan. ¹⁹National Centre for Atmospheric Science, University of Reading, Reading, UK. ²⁰Met Office, Hadley Centre, Exeter, UK. ²¹Climate and Global Dynamics Laboratory, National Center for Atmospheric Research, Boulder, CO, USA. ²²School of Geographical Sciences, University of Bristol, Bristol, UK. ²³Centre for Polar Observation and Modelling, School of Earth and Environment, University of Leeds, Leeds, UK. ²⁴Laboratoire des Sciences du Climat et de l'Environnement, LSCE-IPSL, CEA-CNRS-UVSQ, Université Paris-Saclay, Gif-sur-Yvette, France. ²⁵Lamont-Doherty Earth Observatory, Columbia University, Palisades, NY, USA. ²⁶NASA Goddard Institute for Space Studies, New York, NY, USA. ²⁷Potsdam Institute for Climate Impact Research (PIK), Member of the Leibniz Association, Potsdam, Germany. ²⁸Antarctic Research Centre, Victoria University of Wellington, Wellington, New Zealand. ²⁹Theoretical Division, Los Alamos National Laboratory, Los Alamos, NM, USA. ³⁰Department of Anthropology and Geography, Colorado State University, Fort Collins, CO, USA. ³¹Institute of Low Temperature Science, Hokkaido University, Sapporo, Japan. ³²Department of Earth System Science, University of California Irvine, Irvine, CA, USA. ³³Universities Space Research Association, Goddard Earth Sciences Technology and Research Studies and Investigations, Columbia, MD, USA. ³⁴Laboratory of Climatology, Department of Geography, University of Liège, Liège, Belgium. ³⁵Graduate School of Environmental Studies, Nagoya University, Nagoya, Japan. ³⁶Australian Antarctic Division, Kingston, Tasmania, Australia. ³⁷Australian Antarctic Program Partnership, Institute for Marine and Antarctic Studies, University of Tasmania, Hobart, Tasmania, Australia. ³⁸Arctic Centre, University of Lapland, Rovaniemi, Finland. ³⁹Arctic Research Center, Hokkaido

Article

University, Sapporo, Japan. ⁴⁰Norwegian Polar Institute, Tromsø, Norway. ⁴¹Energy and Climate Group, Department of Physics and Technology, The Arctic University – University of Tromsø, Tromsø, Norway. ⁴²Alfred-Wegener-Institut Helmholtz-Zentrum für Polar- und Meeresforschung, Bremerhaven, Germany. ⁴³Department of Geoscience, University of Bremen, Bremen, Germany. ⁴⁴Laboratory of Hydraulics, Hydrology and Glaciology (VAW), ETH Zurich, Zurich, Switzerland. ⁴⁵Swiss Federal Institute for Forest, Snow and Landscape Research (WSL), Birmensdorf, Switzerland. ⁴⁶Department of Geosciences, University of Fribourg, Fribourg, Switzerland. ⁴⁷Earth System Science and Department Geografie, Vrije Universiteit Brussel, Brussels, Belgium. ⁴⁸Department of Physical Geography, Utrecht University, Utrecht, The Netherlands. ⁴⁹Centre for Polar Observation and Modelling, School of Geographical Sciences, University of Bristol, Bristol, UK. ⁵⁰Atmospheric and Environmental Research, Lexington, MA, USA. ⁵¹GNS Science, Lower Hutt, New Zealand. ⁵²Computational Research Division, Lawrence Berkeley National Laboratory, Berkeley, CA, USA. ⁵³Department of Atmospheric and Cryospheric Sciences, University of Innsbruck, Innsbruck, Austria. ⁵⁴School of Environmental Sciences, University of Liverpool, Liverpool, UK. ⁵⁵Department of Earth, Ocean and Atmospheric Sciences, University of British Columbia, Vancouver, British Columbia, Canada. ⁵⁶Department of Civil and Environmental Engineering, Carnegie Mellon University, Pittsburgh, PA, USA. ⁵⁷Department of Physics and Physical Oceanography, Memorial University of Newfoundland, St John's, Newfoundland, Canada. ⁵⁸Department of Geography, Pennsylvania State University, University Park, PA, USA. ⁵⁹Department of Physics and Astronomy, University of Potsdam, Potsdam, Germany. ⁶⁰Department of Geoscience and Remote Sensing, Delft University of Technology, Delft, The Netherlands. ⁶¹State Key Laboratory of Earth Surface Processes and Resource Ecology, Beijing Normal University, Beijing, China. ⁶²CSC-IT Center for Science, Espoo, Finland. [✉]e-mail: tamsin.edwards@kcl.ac.uk

Methods

Simulations

Ice sheet and glacier model simulations. Ice sheet and glacier simulations are from the Ice Sheet Model Intercomparison Project for CMIP6 (ISMIP6)^{2,3} and GlacierMIP⁴ Phase 2. Most are published elsewhere^{5–8}. Additional ice sheet simulations were included in this analysis (Extended Data Table 1) as follows, where the names are group/model: 22 new Greenland experiments using [5th, 95th] percentile values of the retreat parameter under different climate model forcings with IMAU/IMAUICE1, and 113 Antarctic experiments with CPOM/BISICLES ($N=16$), ILTS_PIK/SICOPOLIS ($N=31$), JPL1/ISSM ($N=10$), LSCE/GRISLI ($N=30$) and NCAR/CISM ($N=26$). Eight of the new Antarctic simulations were previous experiments described in ref.⁷ using a new model (CPOM/BISICLES), and the rest (105) used 37 new combinations of previous uncertainties for additional exploration of basal melt (29) and ice shelf collapse (5) under different climate model forcings, and the interaction of ice shelf collapse and basal melt (3). CPOM/BISICLES is described in the ISMIP6 Antarctic initialization study¹⁵: here the B variant is used, but with minimum resolution 1 km rather than 0.5 km. All ice sheet projections are calculated relative to a control simulation with constant present day climate (see Methods section ‘Comparison with IPCC assessments’ for an estimate of the ‘committed’ contribution this removes).

The glacier regions are listed in Extended Data Table 2 and all simulations are described in ref.⁵. Greenland ice sheet projections have the peripheral glaciers (region 5) masked out, so there is no double-counting. The Antarctic periphery glaciers (region 19) are located only on the surrounding islands, not on the mainland ice sheet; ice sheet models include some of the larger islands, so there is some overlap in area, but the effect of this is estimated to be small (see Methods section ‘Comparison with IPCC assessments’ for an estimate of this and other limitations).

All projections are calculated as annual global mean sea level contributions since 2015, converting mass (for the glaciers) or mass above flotation (for the ice sheets) to sea level contribution using 362.5 Gt per mm SLE.

Global climate model simulations. For building the emulator, we use projections of annual global mean surface air temperature change since 2015 from the CMIP5 and CMIP6 global climate models used to drive the ice sheet and glacier models. If multiple realizations (different initial conditions) for a model were available, we use the mean of these. Data from 1850–2100 were downloaded from the JASMIN/CEDA archive and ESGF on 7 November 2019 and 4 December 2019; the CMIP6 snapshot was updated 28, 29 July 2020. The global mean temperatures used for the projections are described in the section ‘Sea level projections’ below.

Emulation

An emulator is a fast statistical approximation of a computationally expensive simulator. This can be used to predict the simulator response at untried input values—to explore the uncertain input space far more thoroughly—for sensitivity analysis, to adjust the chosen inputs, and to estimate probability distributions. We construct statistical models of the simulated ice sheet and glacier sea level contribution as a function of the global mean surface air temperature of the driving climate models—and also different representations of the ice sheet–ocean interface—to make projections under new emissions scenarios that incorporate these uncertainties, as well as those arising from the different structures of the climate and ice sheet models (and the emulators themselves).

Typically emulation is performed for one model at a time²⁵, but here we emulate each multi-model ensemble all at once. This is made possible by the systematic design of the ISMIP6 and GlacierMIP projects, which

explore uncertainties in global climate change and three ice–ocean parameters simultaneously, and by our approach of applying emulation to multiple models rather than (as is usual) one. The three ice–ocean parameters control: (1) how much Greenland marine-terminating glaciers retreat (κ) with increasing local ocean temperatures and meltwater runoff; (2) how much Antarctic ice shelf basal melting (γ) increases with increasing local ocean temperature; and (3) an on/off scenario of Antarctic ice shelf collapse (C), which can increase glacier flow into the ocean when atmospheric temperatures rise.

We predict the 23 land ice regions separately—the Greenland ice sheet, the West and East Antarctic ice sheets and Antarctic Peninsula, and 19 glacier regions—so the spatial distribution of meltwater can be used in regional sea level projections.

We choose and evaluate emulator structures using the year 2100 (Extended Data Table 2; Extended Data Figs. 1, 2). Global mean surface air temperature projections are taken from the FaIR simple climate model¹², because it can explore uncertainties more thoroughly than the relatively small CMIP6 ensemble of (computationally expensive) general circulation models. We use the same global mean temperature value across all land ice sources for each individual estimate: in other words, we include any co-dependence arising from global temperature. Full details are described in the following sections.

Global mean surface air temperature. Previous sea level emulation studies^{26,27,29,30} have typically used global mean temperature as the main input, rather than regional climate variables. We follow this approach for several reasons: to include correlation of land ice regions induced by global climate change (that is, no need to assume/estimate their correlations, or to treat them as independent), and to have a larger sample of climate change projections. Using regional climate variables would improve the signal-to-noise ratio for the emulator, but would restrict us to using computationally expensive general circulation models from CMIP5/6, for which there only a few tens of models. The simple climate model FaIR can be used to explore uncertainties in each scenario thoroughly, using the latest assessments of equilibrium climate sensitivity.

Global mean temperature is the only regressor for the glacier regions. For the ice sheets, there are additional terms derived from the ISMIP6 parameterizations of ice–ocean interactions.

Ice sheet model parameters. The Greenland glacier retreat parameter κ (Fig. 3a; units $\text{km} (\text{m}^3 \text{s}^{-1})^{-0.4} \text{C}^{-1}$) is a scaling coefficient relating marine-terminating glacier retreat to ocean temperatures and meltwater runoff^{16,17}, where larger negative values indicate greater retreat of the glacier terminus in response to warming. This is a continuous variable, but most simulations use one of three values: the default, which is the median of the distribution in the parameterization¹⁷, $\kappa_{50} = -0.17$, and the quartiles $\kappa_{25} = -0.37$ and $\kappa_{75} = -0.06$. One model uses 5th and 95th percentile values, $\kappa_5 = -0.9705$ and $\kappa_{95} = 0.0079$. For ice sheet models that did not use this parameterization ($N=29$ simulations)⁶, we assign the mean value from the other simulations to minimize the impact on the emulator ($\kappa = -0.2073$). One of these models (BISICLES) also ran ‘high’ and ‘low’ retreat experiments by doubling and halving the ocean thermal forcing, to which we assign the κ_{25} and κ_{75} values.

The Antarctic sub-shelf basal melt parameter γ (Fig. 3b; units of metres per year, m a^{-1}) is the ‘ocean heat exchange velocity’ scaling coefficient relating sub-shelf basal melting to ocean temperatures^{18,19}. Two alternative distributions for γ were derived in the parameterization¹⁹: the first from mean Antarctic melt rates, and the second from the 10 highest observations of melt rate at the grounding line of Pine Island Glacier, where melt rates are currently highest. The values of γ estimated from Pine Island Glacier are an order of magnitude larger, and the two distributions do not overlap. This is a continuous variable, but most simulations use one of three values: the default, which is the median of the mean Antarctic distribution, MeanAnt₅₀ = 14,477, and the 5th and 95th percentiles, MeanAnt₅ = 9,619 and

Article

$\text{MeanAnt}_{95} = 21,005$. Further simulations used the same percentiles from the Pine Island Glacier distribution: $\text{PIG}_{50} = 159,188$, $\text{PIG}_5 = 86,984$ and $\text{PIG}_{95} = 471,264$. Some models⁷ used an alternative variant of the parameterization in which only local ocean temperatures were used, rather than a combination of local and regional, which uses a different tuning for γ . However, the values used are also the 50 [5, 95]th percentiles of those distributions, so we consider them equivalent. For ice sheet models that did not use this parameterization ($N = 62$ simulations), we again assign the ensemble mean value ($\gamma = 59,317$).

The Antarctic ice shelf collapse parameter C is a switch that indicates whether a scenario of ice shelf collapse was used, which can lead to glacier speed-up. A timeline of collapses was derived according to the presence of surface meltwater on ice shelves above a threshold (725 mm a^{-1}) for 10 years, estimated from surface air temperature projections⁴⁵ in the global climate model driving the ice sheet model (mostly CCSM4). This method does not predict whether meltwater may be efficiently drained from the surface for a given ice shelf⁴⁶, thus avoiding collapse. We use values of 1 or 0 indicating whether the scenario is implemented or not.

Gaussian process emulation. Gaussian process emulation⁴⁷ is non-parametric, treating the simulator as an unknown mathematical function of its inputs. We use the R package RobustGaSP⁴⁸ for its numerically robust parameter estimation⁴⁹. There are 23 emulators for the 2100 projections (Greenland ice sheet, three Antarctic ice sheet regions, and 19 glacier regions) and 1,955 emulators for the full land ice time series (23 regions for each year from 2016 to 2100). An alternative to predicting each year separately would be to model the temporal correlation explicitly, but we prefer to use the simpler method, with fewer judgments, and allow temporal correlation to emerge.

Nugget. We use a ‘nugget’ term to incorporate simulations from each multi-model ensemble. The nugget is usually zero for deterministic models—the emulator predicts each simulation in the ensemble exactly, that is, the regression curve goes through all points—or a very small value, to improve numerical stability or other properties^{23,24}. Here we allow the emulator to estimate the nugget, and treat each multi-model ensemble as a set of outputs from a single stochastic simulator or set of noisy observations. This approach has previously been used for emulating stochastic simulators⁵⁰ and for emulating climate models accounting for internal variability, other inert inputs (uncertainties not explicitly modelled in the emulator), and approximations of the model outputs^{51–56}. Our method is similar to the use of ‘emergent constraints’ for climate models^{43,57}, seeking relationships between past and future simulations across multi-model ensembles to constrain them with observations, but here the predictors are inputs to the models rather than their outputs for the past.

This approach does not require the simulations to be normally distributed but does assume they are independent, which has been a long-standing difficulty of interpreting multi-model climate ensembles. But with ice sheet models, although model names may be the same across groups, each one has a very different set up, including physics approximations, parameterizations, tuning, grid resolution, and—in particular—initialization methods, which have been shown to produce very different results even for simulations produced by the same group^{6,7,14,15,58–60}. For glacier models, their structures are also vastly different, ranging from simple scaling parameterizations to dynamic physical models⁵. We test two approaches to account for any model dependence: a dummy variable (see below) and random effects (Methods subsection ‘Antarctic cross-check model’).

Statistical model. Let y denote the simulated global mean sea level contribution for given region and year (in cm SLE), and \mathbf{x} the simulator inputs (see below). Following ref.²³, we write the simulator as a function $y = f(\mathbf{x})$, for which the Gaussian process emulator is described by a mean function:

$$E[f(\mathbf{x})] = h(\mathbf{x})^T \beta,$$

where $h(\mathbf{x})$ is a vector of regression functions, β the corresponding regression coefficients, and where superscript T indicates the transpose; and a covariance function, with variance σ^2 and correlation function $c(\mathbf{x}, \mathbf{x}')$:

$$\text{Cov}[f(\mathbf{x}), f(\mathbf{x}')] = \sigma^2(c(\mathbf{x}, \mathbf{x}') + vI),$$

where v is the nugget term and I the identity matrix. So the prior for $f(\mathbf{x})$ follows a normal distribution:

$$p(f(\mathbf{x}) | \beta, \sigma^2, \delta, v) \sim N(h(\mathbf{x})^T \beta, \sigma^2(c(\mathbf{x}, \mathbf{x}') + vI)),$$

where \mathbf{x} are whichever model inputs are used for a given region, δ are the correlation lengths of the covariance function, and $\sigma^2 v$ is the variability not explained by the inputs. Parameters $(\beta, \sigma^2, \delta, v)$ are estimated from the simulation data.

The inputs \mathbf{x} used in the regression functions are global mean temperature change, T , and, for the ice sheets, the ice–ocean parameter values (k for Greenland; γ , C for Antarctica), plus a dummy variable denoting whether Greenland models used the retreat parameterization. These are discussed in the next section. All inputs are rescaled to have zero mean and unit variance.

Mean functions. The Gaussian process mean function describes the large-scale response of the simulator to its inputs, usually specified as a linear trend with the remainder described by a zero-mean Gaussian process.

For the glaciers, the linear regressor is simply global mean temperature in the same year (T). For the ice sheets, the additional ice sheet model parameters are k for Greenland, and γ and C for Antarctica. We also try two types of dummy variable. The first is for the ice sheet and glacier model names, so these can be treated distinctly in the emulator, but this leads to clear overfitting (that is, the model is too flexible in Figs. 1, 2). The second represents whether an ice sheet model uses the ISMIP6 retreat or basal melt parameterization, to absorb any misalignment between the imputed value and the effective value. Bayesian information criterion (BIC) from a stepwise model selection (testing up to first-order interactions) suggests this dummy variable is informative for Greenland, so we retain it (o , for open parameterization), but not for the Antarctic regions. The stepwise model selection suggests we could reasonably include terms for the interaction between temperature and retreat for Greenland, temperature and basal melt for West Antarctica, and temperature and collapse for East Antarctica, but we choose not to, to avoid the risk of overfitting. The selection also shows that collapse strongly dominates the Antarctic Peninsula response, and may not be needed for West Antarctica, but we retain all terms (that is, T_i, γ, C) because we otherwise find the covariance matrix is poorly conditioned. The resulting mean functions are $h_{\text{GrIS}}(\mathbf{x})_i \sim (T_i, k, o)$ for Greenland, $h_{\text{AIS}}(\mathbf{x})_i \sim (T_i, \gamma, C)$ for the Antarctic regions, and $h_{\text{Glaciers}}(\mathbf{x})_i \sim (T_i)$ for the glaciers, where $h - (a, b)$ means h is a linear function of a and b , and i is the index for the year.

Covariance functions. The covariance function describes the smoothness of the Gaussian process. As in any statistical modelling, there is a trade-off between improving accuracy and over-fitting. We assess this using the usual leave-one-out procedure^{61,62}. We fit the emulator to all ensemble members but one, then predict the sea level contribution from this simulation; we repeat this for every combination, noting the emulator error (residual) and uncertainty for each prediction. We perform this for each of the 23 regional emulators for the year 2100 with five covariance functions of varying smoothness—Matérn(5/2), which is the default in RobustGaSP, Matérn (3/2), and three members of the power exponential family with high, medium

and low exponent values ($\alpha=1.9$, that is, close to a squared exponential, the default value; $\alpha=1.0$, exponential; and $\alpha=0.1$, for which the covariance function has a small effect so the emulator approaches linear regression).

For 18 of the 19 glacier regions, we use the covariance function with the smallest standardized Euclidean distance between the emulator predictions and simulations (standardized because, unlike simpler metrics such as root-mean-square error or mean absolute error, it does not penalize larger errors if the emulator uncertainty intervals are sufficiently large), as in ref.²⁵. For the Southern Andes (region 17), all covariance functions give identical distances, so we use the default for RobustGaSP. For the ice sheets, we use the covariance function that gives close to linear regression (power exponential, $\alpha=0.1$), rather than the one with the minimum Euclidean distance, for various reasons. For Greenland, West Antarctica and the Antarctic Peninsula, the minimum distance covariance functions (power exponential $\alpha=1.0$ for Greenland; Matérn(3/2) for the Antarctic regions) result in overfitting for temperature (that is, too much flexibility in Fig. 1). For East Antarctica, the minimum distance covariance functions (Matérn(5/2)) result in an incorrect sign prediction under the ice shelf collapse switch. Using the alternative covariance function solves all of these issues and does not increase the standardized Euclidean distance by much: 4% for the Peninsula, and 0.4%–1% for the other three regions. The resulting covariance function choices are given in Extended Data Table 2.

Evaluating the emulators. After selecting the covariance functions for each regional emulator at 2100, we evaluate the emulators further by plotting the emulator predictions against the simulations from the leave-one-out procedure, and the standardized residuals (the difference between the emulator prediction and the simulator, divided by the emulator standard deviation), and calculating the percentage of simulations falling within ± 2 s.d. (Extended Data Table 2 and Extended Data Figs. 1, 2). We would not expect exactly 95% of the simulations to fall within 2 s.d., in part because the predictions are not independent, but very low or high values would suggest emulator over- or under-confidence. The region with the lowest percentage of predictions within the uncertainty intervals is North Asia (region 10) with 89%, indicating slightly too small emulator uncertainty estimates, and the highest is 98% (Scandinavia, region 8), indicating the reverse.

Mean absolute errors for each emulator are given in Extended Data Table 2 and Extended Data Figs. 1, 2: for the ice sheet regions they are 0.28 cm (Peninsula), 1.4 cm (Greenland) and 1.5 cm (East Antarctica) and 2.0 cm (West Antarctica), and for the individual glacier regions they range from 0.0020 cm to 0.87 cm (Antarctic periphery, region 19). Mean absolute standardized errors are all less than 0.006.

The emulator underestimates the three to four highest West and East Antarctic contributions by around 10–15 cm (Extended Data Fig. 1b, c). The five highest of these are from the SICOPOLIS model, which has a much greater sensitivity to basal melting than other models (see main text, Methods subsection ‘Robustness checks’ and Extended Data Fig. 6), and use the highest value of this parameter ($\gamma = \text{PIG}_{95}$). These simulations are therefore extreme: 1% of the 344 simulations, and the 97.5th percentile value of the basal melt parameter. There are process-based reasons to expect that SICOPOLIS is an upper bound or overestimate (see main text). When the emulator is calibrated with this model alone, it does not underestimate its highest contributions (not shown). The resulting projections under the NDC scenario are shown in Methods subsection ‘Robustness checks’ (test 4); the difference with the main projections may be interpreted as the maximum possible impact of this emulator underestimate, if SICOPOLIS were the sole realistic ice sheet model. These are lower than the ‘risk-averse’ projections, which are made with a subset of high sensitivity ice sheet models and other pessimistic assumptions (see main text).

We therefore consider the emulators to be adequate for the predictions of large-scale sea level contribution presented here.

Antarctic cross-check model. We perform a cross-check for the Antarctic ice sheet regions at 2100 using a linear mixed model, with the ice sheet model name included as a random effect to deal with any systematic uncertainty arising from dependence of ensemble members. This attributes some of the uncertainty in the response to the ice sheet model used, and this uncertainty can then be removed from the predicted probability density function (PDF). We thus model the ensemble members as ‘similar but not identical’, using a mean function of temperature and ice sheet parameters, plus a structured error term that includes a systematic component according to the ice sheet model and a noise component to capture other sources of variability such as initialization.

For the mean function (also linear), we use the logarithm of y as a regressor, so it is always positive. Consequently we use the geometric mean as the missing value, rather than the arithmetic mean. We use a dummy variable to denote these models, as for Greenland in the Gaussian process emulator. The full global mean temperature change trajectories are used instead of only the total change at 2100. To increase the signal-to-noise ratio, the annual means are reduced to decadal means (2015–2029, 2030–2039, ..., 2090–2100). There are 13 distinct forcings, each one the product of a global climate model and a scenario, so we represent the forcing variables as 12 bisquare basis functions. These start as 13 bisquare basis functions, each one centred at one of the 13 forcings, but one is dropped because otherwise the model matrix becomes rank deficient when a constant is added. The one dropped is the one with the smallest mean Euclidean distance to the other 12. We use bisquare kernels, where the standard deviation of each kernel is set to one-tenth of the maximum Euclidean distance between all pairs of forcings, to cover the forcing space with non-zero values for the forcing regressors. We use the same distributions for temperature, basal melt and collapse as the main projections, and set the dummy variable to represent standard parameterization models.

This emulator predicts 50 [5, 95]th percentiles for the West Antarctic sea level contribution at 2100 of 2 [−4, 8] cm SLE for SSP1-26 and 3 [−4, 10] cm SLE for SSP5-85, which are very similar to the Gaussian process emulator predictions of 2 [−5, 10] cm SLE and 3 [−4, 11] cm SLE. We test the effect of changing the kernel standard deviation to one-twelfth or one-fourteenth of the maximum Euclidean distance; the largest change is a 2-cm decrease in the 95th percentile under SSP5-85. For East Antarctica, the emulator with random effects predicts 2 [−3, 6] cm SLE for both scenarios; the Gaussian process emulator predicts a small scenario dependence, 2 [−4, 7] cm SLE for the low emissions scenario and 0 [−5, 6] cm SLE for the high. For the Antarctic Peninsula, the random effects predictions are 0 [−1, 2] cm SLE for both scenarios, and the Gaussian process predictions are the same. These similarities give us confidence that model dependence is not substantially affecting our projections—that is, that differences in model structure, resolution, calibration and initialization dominate over the similarities—although it would be worth investigating this in more detail.

Sea level projections

We use probability distributions for global temperature and the ice sheet model parameters as inputs to each emulator to make the projections.

Global mean temperature projections. We use projections of global annual mean surface air temperature change since 2015 from the FaIR (Finite amplitude Impulse Response) simple climate model for the main projections. We take the 500-member ensemble from ref.¹²: SSP1-19, SSP1-26, SSP3-70, SSP5-85 and a scenario estimated for the 2019 NDCs. We also use projections for SSP2-45 generated with the same ensemble.

Ice sheet model parameter distributions. For Greenland, we sample from a kernel density estimate of the original κ distribution ($N=191$)

Article

with the same bandwidth used in deriving the parameterization^{16,17} ($N=0.0703652$) (Fig. 1b). The dummy variable is always set to represent the standard ISMIP6 parameterization.

For Antarctica, we combine the mean Antarctic and Pine Island Glacier γ distributions ($N=10,000$ each), and sample from a kernel density estimate using three times the automatic bandwidth (Silverman's 'rule of thumb')⁶³ to merge and smooth them into a near-unimodal distribution that we truncate at zero (Fig. 1c). For the collapse switch C , we sample randomly from 0 or 1 with equal probability (8% of the ISMIP6 simulations have ice shelf collapse). The ice shelf collapse scenario does not include the possibility of surface meltwater draining efficiently from some ice shelves under certain conditions, thereby avoiding collapse, so we feel this is a reasonable judgement.

Sampling. For the 2100 projections, we sample from the FaIR ensemble ($N=500$) with replacement ($N=5,000$ for main and risk-averse projections; $N=1,000$ for robustness and sensitivity tests). For the full time series, we use the 500 FaIR projections directly without resampling. We make one set of emulator predictions (23 regions) for each temperature value in a given year, randomly sampling the relevant ice–ocean parameters (k, γ, C) once for each FaIR ensemble member.

We integrate over the uncertain inputs (temperature in a given year, and ice–ocean parameters) to obtain the final probability density functions (PDFs). Each regional emulator predicts a Student's t test distribution for a given set of these input values, defined by a mean and standard deviation; we approximate this with a normal distribution, as in refs.^{54,56}, which is accurate enough for this application. We use different integration methods for the 23 individual regional PDFs compared with the regional sums (Antarctica, global glaciers, and land ice total). For the individual regional estimates, we use deterministic numerical integration (the midpoint rule: we sum the Gaussian distributions for each emulator prediction, then normalize). For regional sums we must use Monte Carlo sampling, because the three ice sources (Greenland, Antarctica and glaciers) have different parameters, and we also desire traceability of predictions to input values within a given ice source. We sample once from the Gaussian distribution for each emulator prediction, then sum the regional samples for a given temperature to estimate the PDF, smoothing with kernel density estimation for figures (again using Silverman's 'rule of thumb'⁶³ for the bandwidth). Sampling is a more noisy method of integration than deterministic methods, so the PDFs for regional sums are less smooth than those for individual regions.

Glacier maximum cap. We apply a cap to the glacier projections using estimates of their maximum sea level contribution⁴⁴. Glacier model projections often exceed this cap in some regions, if near or total loss is projected under high emissions, either because they report changes in total mass, not mass above flotation, or because of errors in initial mass⁵, or both. We restrict values to the maximum in the emulator mean predictions and then the PDFs (the latter exceeding the cap owing to emulator uncertainty).

Time-series smoothing. Interannual variability arises in the time series owing to sampling the emulator uncertainty for each annual regional prediction. We apply a five-year running mean in Fig. 3d to visualize the expected smoothness of sea level contributions.

Comparison with IPCC assessments

The ice sheet projections are made relative to control simulations with a constant recent climate. This control includes both the model drift and, depending on the initialization method, any background contribution arising from forcing before 2015. This background contribution should be added to the ice sheet projections, but is difficult to quantify. Five-year mean rates of sea level contribution since 1992/3 range from 0.1–0.8 mm yr⁻¹ for the Greenland ice sheet⁶⁴ and 0.1–0.6 mm yr⁻¹

for Antarctica⁶⁵, but they would decrease in the absence of forcing after 2014. Modelling work to quantify the background contribution from Greenland⁶⁶ suggests a contribution of 0.6 ± 0.2 cm SLE by 2100. Estimates made for this study range from 0.3–0.8 cm under a range of retreat parameter values, $\kappa_{75} - \kappa_{25}$ (IMAU/IMAUICE1: 0.3–0.4 cm; CISM variant similar to NCAR/CISM: 0.4–0.8 cm). For Antarctica, the dynamic commitment has been estimated to be 2 cm SLE at 2100 for the Amundsen Sea Embayment region of West Antarctica, where most mass loss is currently occurring⁶⁷. Part of these trends may still be due to residual model drift. The committed contribution could therefore add up to ~1 cm per century to our Greenland projections and ~2 cm per century to the Antarctic.

The Antarctic ice sheet models include some of the larger islands that are also included in region 19, potentially leading to double-counting. However, median projections for region 19 range from 1–2 cm under different emissions scenarios, and the ice sheet models are much lower resolution (that is, the glaciers are probably less responsive), so the effect is expected to be of order 0.5–1 cm SLE or less.

We average our projections over the 86 years and compare them with the average IPCC AR5²⁶ and SROCC¹ projections over 95 years (the midpoints of 1986–2005 to 2081–2100) as rates of cm SLE per century. For the glaciers, we project 8 cm per century SLE for SSP1-26 and 16 cm per century for SSP5-85 excluding the Antarctic peripheral glaciers (region 19: 1 cm and 2 cm, respectively), compared with 10 cm for RCP2.6 and 17 cm for RCP8.5 in AR5. For the Greenland ice sheet, we project 4 cm per century SLE for SSP1-26 and 11 cm for SSP5-85, compared with 6 cm for RCP2.6 and 13 cm for RCP8.5 in AR5. For Antarctica, we project 5 cm per century SLE for both scenarios; the AR5 projections are 5 cm per century SLE for RCP2.6 and 4 cm for RCP8.5, whereas those for SROCC are 4 cm per century SLE for RCP2.6 and 11 cm for RCP8.5. The difference between scenarios for Antarctica in AR5 arises only from additional accumulation, because the dynamic contributions are assumed to be the same.

Glacier projections could be overestimated because meltwater routing to the ocean is not accounted for (not all volume lost from the glaciers reaches the oceans), or underestimated because only one glacier model includes ice–water interactions (that is, frontal ablation of marine- and lake-terminating glaciers). For the latter, we compare mean projections for the GloGEM model to the emulator for RCP8.5/SSP5-85 and RCP4.5/SSP2-45 for key regions, and find they are larger by less than 1 cm for Alaska and Russian Arctic (regions 1 and 9), by less than 0.5 cm for Svalbard (7) and Arctic Canada South (4), and smaller than the emulator for Arctic Canada North (3). All are within the emulator 95th-percentile estimates. We may slightly underestimate uncertainty in the global glacier total owing to correlated errors across models⁵ by emulating the regions independently, though there are compensating advantages (more accurate emulation, spatial pattern of meltwater); a similar argument applies to Antarctica.

Sensitivity tests

We perform a number of checks to test the sensitivity of the ice sheet projections to changes in the chosen inputs: predominantly the input distributions, but also the dataset in the final test (see Extended Data Table 3 and refs.^{12,26,27,33,38}). All results are shown for the SSP5-85 scenario in Extended Data Fig. 4 under the index given (where 1 is the main projection); numerical values in the text refer to changes in the median and [5, 95]th percentile estimates for the ice sheet under this scenario unless otherwise stated.

Robustness checks

We perform a number of checks to test robustness of the ice sheet projections to changes in the simulation dataset (see Extended Data Table 4 and refs.^{6,8,25,65}). Results are shown for the NDCs scenario in Extended Data Fig. 5 under the test index given (where 1 is the main projection); numerical values in the text refer to changes in the median

and [5, 95]th percentile estimates under this scenario unless otherwise stated. The full datasets are 256 simulations for Greenland and 344 simulations for Antarctica.

Parameter interactions

Retreat and basal melt versus temperature. Ice sheet projection uncertainties are constant across scenarios. However, tests with three ice sheet models show that the range of projections from high to low values of the retreat parameter ($K_{95} - K_5$) and basal melt parameter (PIG₉₅ – MeanAnt₅₀) is consistently smaller under RCP2.6 than under RCP8.5, so the emulator uncertainty should be smaller at lower temperatures. The ratios of ranges, RCP2.6/RCP8.5, for each group/model + GCM are as follows.

Greenland. IMAU/IMAUICE + MIROC5 = 1.4097/8.3069 = 0.17; IMAU/IMAUICE + CNRM-CM6-1 = 2.4813/9.7187 = 0.26.

West Antarctica. JPL1/ISSM + NorESM1-M = 0.40; CPOM/BISICLES + NorESM1-M = 0.57.

East Antarctica. JPL1/ISSM + NorESM1-M = 0.73; CPOM/BISICLES + NorESM1-M = 0.32.

The emulator does not have sufficient data from lower emissions scenarios to reduce the variance, particularly for Greenland. If other ice sheet models respond the same way as the above, then adding more simulations may reduce the uncertainty for low SSPs.

Ice shelf collapse versus basal melt. The contribution due to ice shelf collapse does not increase with higher values of the basal melt parameter in the models JPL1/ISSM and CPOM/BISICLES (0.1 cm difference for the Peninsula in BISICLES; all other regional differences for both models ≤ 0.02 cm).

Data availability

All global climate, simple climate, ice sheet and glacier model data used as inputs to this study are provided with the code as described above. Main and risk-averse projections at 2100 from the analysis are provided in Supplementary Information for each of the 23 regions, and the Antarctic, glacier and land ice sums.

Code availability

R code and input data are available at <https://github.com/tamsinedwards/emulandice>. Each simulation in the sea level projections file has a label in the ‘publication’ column for the reference (Goelzer2020⁶, Seroussi2020⁷, Payne2021⁸ or Marzeion2020⁹), or ‘New’ if previously unpublished.

45. Trusel, L. D. et al. Divergent trajectories of Antarctic surface melt under two twenty-first-century climate scenarios. *Nat. Geosci.* **8**, 927–932 (2015).
46. Bell, R. E. et al. Antarctic ice shelf potentially stabilized by export of meltwater in surface river. *Nature* **544**, 344–348 (2017).
47. O'Hagan, A. Bayesian analysis of computer code outputs: a tutorial. *Reliab. Eng. Syst. Saf.* **91**, 1290–1300 (2006).
48. Gu, M. et al. RobustGaSP: robust Gaussian stochastic process emulation in R. *R J.* **11**, 112–136 (2019).
49. Gu, M., Wang, X. & Berger, J. O. Robust Gaussian stochastic process emulation. *Ann. Stat.* **46**, 3038–3066 (2018).
50. van Beers, W. C. M. & Kleijnen, J. P. C. Kriging for interpolation in random simulation. *J. Oper. Res. Soc.* **54**, 255–262 (2003).
51. Salter, J. M. & Williamson, D. A comparison of statistical emulation methodologies for multi-wave calibration of environmental models. *Environmetrics* **27**, 507–523 (2016).
52. Williamson, D. & Blaker, A. T. Evolving Bayesian emulators for structured chaotic time series with application to large climate models. *SIAM/ASA J. Uncertain. Quant.* **2**, 1–28 (2014).
53. Williamson, D., Blaker, A., Hampton, C. & Salter, J. Identifying and removing structural biases in climate models with history matching. *Clim. Dyn.* **45**, 1299–1324 (2015).
54. Araya-Melo, P. A., Crucifix, M. & Bounceur, N. Global sensitivity analysis of the Indian monsoon during the Pleistocene. *Clim. Past* **11**, 45–61 (2015).
55. Bounceur, N., Crucifix, M. & Wilkinson, R. D. Global sensitivity analysis of the climate–vegetation system to astronomical forcing: an emulator-based approach. *Earth Syst. Dynam.* **6**, 205–224 (2015).
56. Lord, N. S. et al. Emulation of long-term changes in global climate: application to the late Pliocene and future. *Clim. Past* **13**, 1539–1571 (2017).
57. Bowman, K. W. et al. A hierarchical statistical framework for emergent constraints: application to snow–albedo feedback. *Geophys. Res. Lett.* **45**, 13050–13059 (2018).
58. Nowicki, S. et al. Insights into spatial sensitivities of ice mass response to environmental change from the SeaRISE ice sheet modeling project. I: Antarctica. *J. Geophys. Res. Earth* **118**, 1002–1024 (2013).
59. Nowicki, S. et al. Insights into spatial sensitivities of ice mass response to environmental change from the SeaRISE ice sheet modeling project. II: Greenland. *J. Geophys. Res. Earth* **118**, 1025–1044 (2013).
60. Saito, F., Abe-Ouchi, A., Takahashi, K. & Blatter, H. SeaRISE experiments revisited: potential sources of spread in multi-model projections of the Greenland ice sheet. *Cryosphere* **10**, 43–63 (2016).
61. Rougier, J., Sexton, D. M. H., Murphy, J. M. & Stainforth, D. A. Analyzing the climate sensitivity of the HadSM3 climate model using ensembles from different but related experiments. *J. Clim.* **22**, 3540–3557 (2009).
62. Bastos, L. S. & O'Hagan, A. Diagnostics for Gaussian process emulators. *Technometrics* **51**, 425–438 (2009).
63. Silverman, B. W. *Density Estimation* (Chapman and Hall, 1986).
64. The IMBIE Team. Mass balance of the Greenland Ice Sheet from 1992 to 2018. *Nature* **579**, 233–239 (2020).
65. The IMBIE Team. Mass balance of the Antarctic Ice Sheet from 1992 to 2017. *Nature* **558**, 219–222 (2018).
66. Price, S. F., Payne, A. J., Howat, I. M. & Smith, B. E. Committed sea-level rise for the next century from Greenland ice sheet dynamics during the past decade. *Proc. Natl Acad. Sci. USA* **108**, 8978–8983 (2011).
67. Aleypopoulos-Borrelli, A. V., Nias, I. J., Payne, A. J., Golledge, N. R. & Bingham, R. J. Ocean-forced evolution of the Amundsen Sea catchment, West Antarctica, by 2100. *Cryosphere* **14**, 1245–1258 (2020).

Acknowledgements We thank J. Rougier for providing advice and support throughout, and writing the original random effects model. We also thank B. Fox-Kemper, H. Hewitt, R. Kopp, S. Drijfhout and J. Rohmer for discussions, suggestions and support. We thank N. Barrand, W. Chang, V. Volodina and D. Williamson for their thorough and constructive comments, which greatly improved the manuscript. We thank the Climate and Cryosphere (CliC) Project, which provided support for ISMIP6 and GlacierMIP through sponsoring of workshops, hosting the websites and ISMIP6 wiki, and promotion. We acknowledge the World Climate Research Programme, which, through its Working Group on Coupled Modelling, coordinated and promoted CMIP5 and CMIP6. We thank the climate modelling groups for producing and making available their model output, the Earth System Grid Federation (ESGF) for archiving the CMIP data and providing access, the University at Buffalo for ISMIP6 data distribution and upload, and the multiple funding agencies who support CMIP5 and CMIP6 and ESGF. We thank the ISMIP6 steering committee, the ISMIP6 model selection group and the ISMIP6 dataset preparation group for their continuous engagement in defining ISMIP6. This is ISMIP6 contribution no. 13. This publication was supported by PROTECT, which has received funding from the European Union's Horizon 2020 research and innovation programme under grant agreement no. 869304. This is PROTECT contribution number 12. T.L.E. was supported by PROTECT and the UK Natural Environment Research Council grant NE/T007443/1. F.T. was supported by PROTECT. J.F.O.N. was supported by the UK Natural Environment Research Council London Doctoral Training Partnership. R. Gladstone's contribution was supported by Academy of Finland grants 286587 and 322430, and T. Zwinger's by grant 322430. W.H.L. and G.R.L. were supported by the National Center for Atmospheric Research, which is a major facility sponsored by the National Science Foundation under Cooperative Agreement no. 1852977. Computing and data storage resources for CISM simulations, including the Cheyenne supercomputer (<https://doi.org/10.5065/D6RX99HX>), were provided by the Computational and Information Systems Laboratory (CISL) at NCAR. Support for X.A.-D., M.J.H., S.F.P. and T. Zhang was provided through the Scientific Discovery through Advanced Computing (SciDAC) programme funded by the US Department of Energy (DOE), Office of Science, Advanced Scientific Computing Research and Biological and Environmental Research programmes. N.R.G., D.P.L. and B.A. were supported by New Zealand Ministry for Business, Innovation and Employment contracts RTUV1705 ('NZSeaRise') and ANTA1801 ('Antarctic Science Platform'). J.M.G. and R.S.S. were supported by the National Centre for Atmospheric Science, funded by the UK National Environment Research Council. R. Calov was funded by the PalMod project of the Bundesministerium für Bildung und Forschung (BMBF) with the grants FKZ 01LP1502C and 01LP1504D. D.F.M. and C.S. were supported by the Director, Office of Science, Offices of Advanced Scientific Computing Research (ASCR) and Biological and Environmental Research (BER), of the US Department of Energy under contract no. DE-AC02-05CH1231, as a part of the ProSPect SciDAC Partnership. BISICLES simulations used resources of the National Energy Research Scientific Computing Center (NERSC), a US Department of Energy Office of Science User Facility operated under contract no. DE-AC02-05CH1231. C.Z. and B.K.G.-F. were supported under the Australian Research Council's Special Research Initiative for Antarctic Gateway Partnership (project ID SR140300001) and received grant funding from the Australian Government for the Australian Antarctic Program Partnership (project ID ASCI000002). Work was performed by E.L., N.-J.S. and H.S. at the California Institute of Technology's Jet Propulsion Laboratory under a contract with the National Aeronautics and Space Administration; support was provided by grants from NASA's Cryospheric Science, Sea Level Change Team, and Modeling, Analysis and Prediction (MAP) programmes. They acknowledge computational resources and support from the NASA Advanced Supercomputing Division. The CMIP5 and CMIP6 projection data were processed by C.M.M. with funding from the European Union's CONSTRAIN project as part of the Horizon 2020 Research and Innovation Programme under grant agreement number 820829. A. Barthel was supported by the DOE Office of Science HiLAT-RASM project and Early Career Research programme. T.A. and R.W. are supported by the Deutsche Forschungsgemeinschaft (DFG) in the framework of the priority programme 'Antarctic research with comparative investigations in Arctic ice areas' by grants WI4556/2-1 and WI4556/4-1, and within the framework of the PalMod project (FKZ: 01LP1925D) supported by the German Federal Ministry of Education and Research (BMBF) as a Research for Sustainability initiative (FONA). R.R. is supported by the Deutsche Forschungsgemeinschaft (DFG) by grant WI4556/3-1 and through the TiPACCs

Article

project that receives funding from the European Union's Horizon 2020 Research and Innovation programme under grant agreement no. 820575. Development of PISM is supported by NASA grant NNX17AG65G and NSF grants PLR-1603799 and PLR-1644277. The authors gratefully acknowledge the European Regional Development Fund (ERDF), the German Federal Ministry of Education and Research and the Land Brandenburg for supporting this project by providing resources for the high-performance computer system at the Potsdam Institute for Climate Impact Research. Computer resources for this project have also been provided by the Gauss Centre for Supercomputing, Leibniz Supercomputing Centre (<http://www.lrz.de>, last access: 16 July 2020) under project IDs pr94ga and pn69ru. R. Greve and C.C. were supported by Japan Society for the Promotion of Science (JSPS) KAKENHI grant nos JP16H02224 and JP17H06323. R. Greve was supported by JSPS KAKENHI grant no. JP17H06104, by a Leadership Research Grant of Hokkaido University's Institute of Low Temperature Science (ILTS), and by the Arctic Challenge for Sustainability (ArCS, ArCS II) project of the Japanese Ministry of Education, Culture, Sports, Science and Technology (MEXT) (programme grant nos JPMXD1300000000, JPMXD1420318865). F.P. and S. Sun were supported by the MIMO project within the STEREO III programme of the Belgian Science Policy Office, contract SR/00/336 and the Fonds de la Recherche Scientifique (FNRS) and the Fonds Wetenschappelijk Onderzoek-Vlaanderen (FWO) under the EOS project no. O0100718F. A. Shepherd was supported by the UK Natural Environment Research Council in partnership with the Centre for Polar Observation and Modelling and the British Antarctic Survey and by the European Space Agency Climate Change Initiative. D.F. was supported by an appointment to the NASA Postdoctoral Program at the NASA Goddard Space Flight Center, administered by Universities Space Research Association under contract with NASA. R.v.d.W. acknowledges the support of the Future Deltas programme of Utrecht University. C.J.S. was supported by a NERC/IIASA Collaborative Research Fellowship (NE/T009381/1). H.G. has received funding from the programme of the Netherlands Earth System Science Centre (NESSC), financially supported by the Dutch Ministry of Education, Culture and Science (OCW) under grant no. 024.002.001 and from the Research Council of Norway under projects INES (270061) and KeyClim (295046). F.S. acknowledges support from DOE Office of Science grant no. DE-SC0020073. High-performance computing and storage resources were provided by the Norwegian Infrastructure for Computational Science through projects NN9560K, NN9252K, NS9560K, NS9252K and NS501K.

Author contributions T.L.E. conceived the idea, carried out all statistical analysis except the random effects model, produced the figures, and wrote the manuscript. S.N. led ISMIP6, including experimental design, organization and analysis, and provided scientific interpretation. B.M. and R.H. co-led GlacierMIP and contributed simulations (below), and provided data and interpretation. H.G. and H.S. led the processing and analysis in ISMIP6 for the Greenland and Antarctic ice sheets, respectively, contributed simulations (below), and provided scientific interpretation and advice. N.C.J. and D.A.S. co-derived with T.L.E. the ice sheet continuous parameter distributions for the emulator, and also derived the corresponding ocean forcing parameterization studies with X.A.-D., F.S. and T.H. for Antarctica and with F.S., D.F. and M.M. for Greenland. F.T. performed the random effects model cross-check for Antarctica. C.J.S. provided the FaIR projections and C.M.M. provided the CMIP5 and CMIP6

projection data for the emulator. E.S. led the ISMIP6 data processing. A.A.-O., J.M.G., E.L., W.H.L., A.J.P., A. Shepherd contributed to the ISMIP6 experimental design, organization and analysis as members of its steering committee, and R.S.S. and W.H.L. led the ISMIP6 atmosphere focus group. C.M.L., A. Barthel and C.A. selected the CMIP5 models for ISMIP6, X.F. and P.A. ran the surface mass balance model for the Greenland and R. Cullather prepared the Antarctic surface mass balance, and L.D.T. and M.v.d.B. provided the ice shelf collapse forcing. For Antarctica: T.K. and A.H. contributed the AWI/PISM simulations; M.J.H., T. Zhang and S.F.P. contributed the DOE/MALI simulations; R. Greve and R. Calov contributed the ILTS_PIK/SICOPOLIS simulations; H.G. and R.v.d.W. contributed the IMAU/IMAUICE simulations; N.-J.S. and H.S. contributed the JPL/ISSM simulations; C.D. and A.Q. contributed the LSCE/GRISLI simulations; G.R.L. and W.H.L. contributed the NCAR/CISM simulations; R.R., T.A. and R.W. contributed the PIK/PISM simulations; T.P., M.M. and H.S. contributed the UCJPL/ISSM simulations; F.P. and S. Sun contributed the ULB/fETISH simulations; C.Z., R. Gladstone, B.K.G.-F. and T. Zwinger contributed the UTAS/Elmer/Ice simulations; J.V.B. and P.H. contributed the VUB/AISMPALEO simulations; N.R.G. and D.P.L. contributed the VUW/PISM simulations; and D.F.M., C. Shafer and J.F.O.N. contributed the CPOM/BISICLES simulations. For Greenland: M.R. and A.H. contributed the AWI/ISSM simulations; V.L. and A.J.P. contributed the BGC/BISICLES simulations; I.N., D.F. and S.N. contributed the GSFC/ISSM simulations; R. Greve, R. Calov and C.C. contributed the ILTS_PIK/SICOPOLIS simulations; H.G., R.v.d.W. and M.v.d.B. contributed the IMAU/IMAUICE simulations; N.-J.S. and H.S. contributed the JPL/ISSM simulations; J.C. and N.-J.S. contributed the JPL/ISSMPALEO simulations; A.Q. and C.D. contributed the LSCE/GRISLI simulations; L.T. contributed the MUN/GSM simulations; W.H.L. and G.R.L. contributed the NCAR/CISM simulations; A.A. contributed the UAF/PISM simulations; Y.C., H.S. and M.M. contributed the UCJPL/ISSM simulations; S.L.C. and P.H. contributed the VUB/GISM simulations; and D.P.L. and N.R.G. contributed the VUW/PISM simulations. For global glaciers: B.A. contributed the AND2012 simulations; K.F. and A. Sakai contributed the GLIMB simulations; M. Huss contributed the GloGEM simulations; H.Z. contributed the GloGEMflow simulations; S. Shannon contributed the JULES simulations; P.K. and W.I. contributed the KRA2017 simulations; B.M. and J.-H.M. contributed the MAR2012 simulations; F.M. and N.C. contributed the OGGM simulations; D.R.R. and R.H. contributed the PyGEM simulations; A. Bliss and V.R. contributed the RAD2014 simulations; R.v.d.W. contributed the WAL2001 simulations; and A. Bliss and J.-H.M. assisted with data handling. All authors contributed to the manuscript.

Competing interests The authors declare no competing interests.

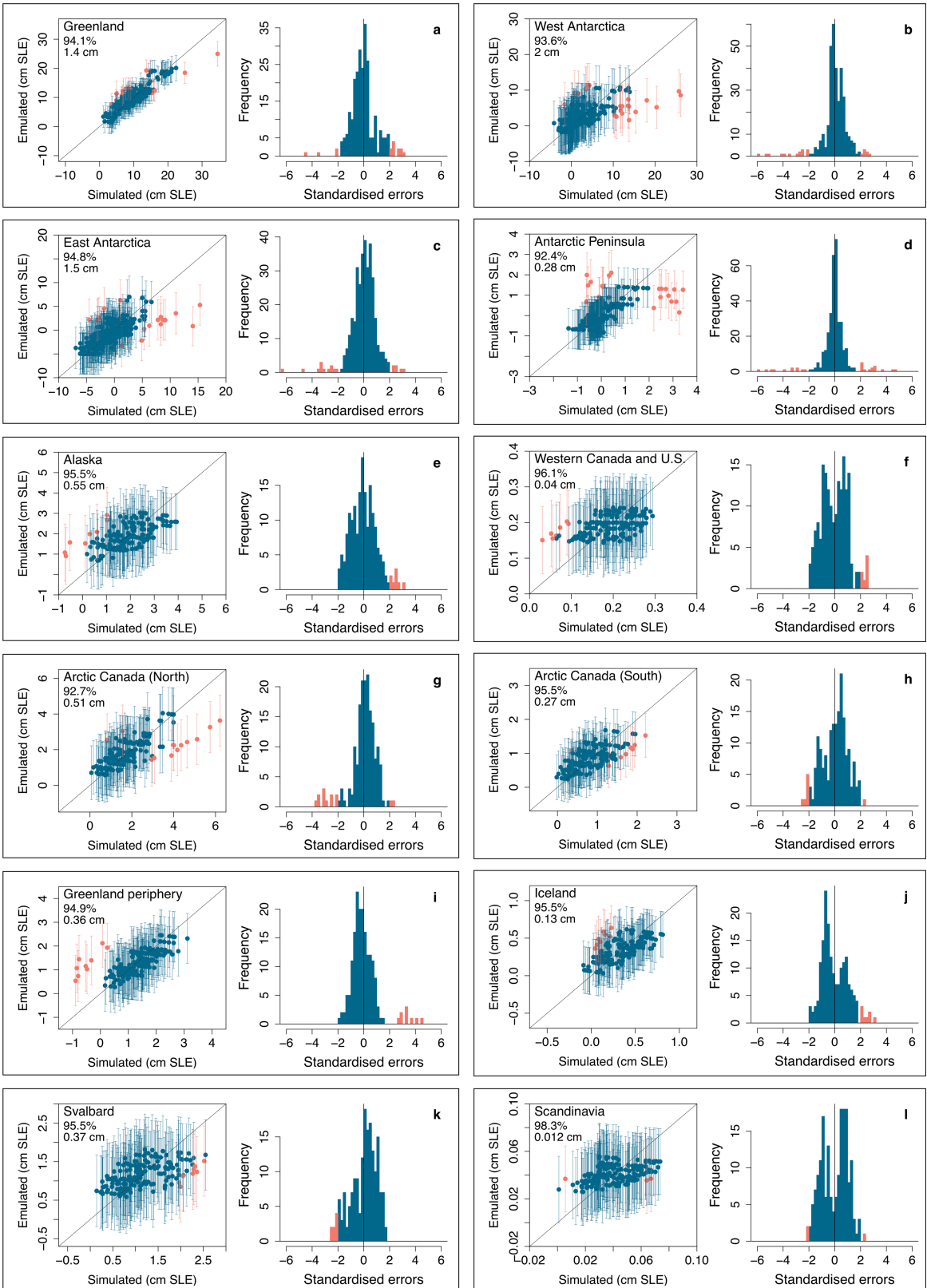
Additional information

Supplementary information The online version contains supplementary material available at <https://doi.org/10.1038/s41586-021-03302-y>.

Correspondence and requests for materials should be addressed to T.L.E.

Peer review information *Nature* thanks Nicholas Barrand, Won Chang, Victoria Volodina, Daniel Williamson and the other, anonymous, reviewer(s) for their contribution to the peer review of this work.

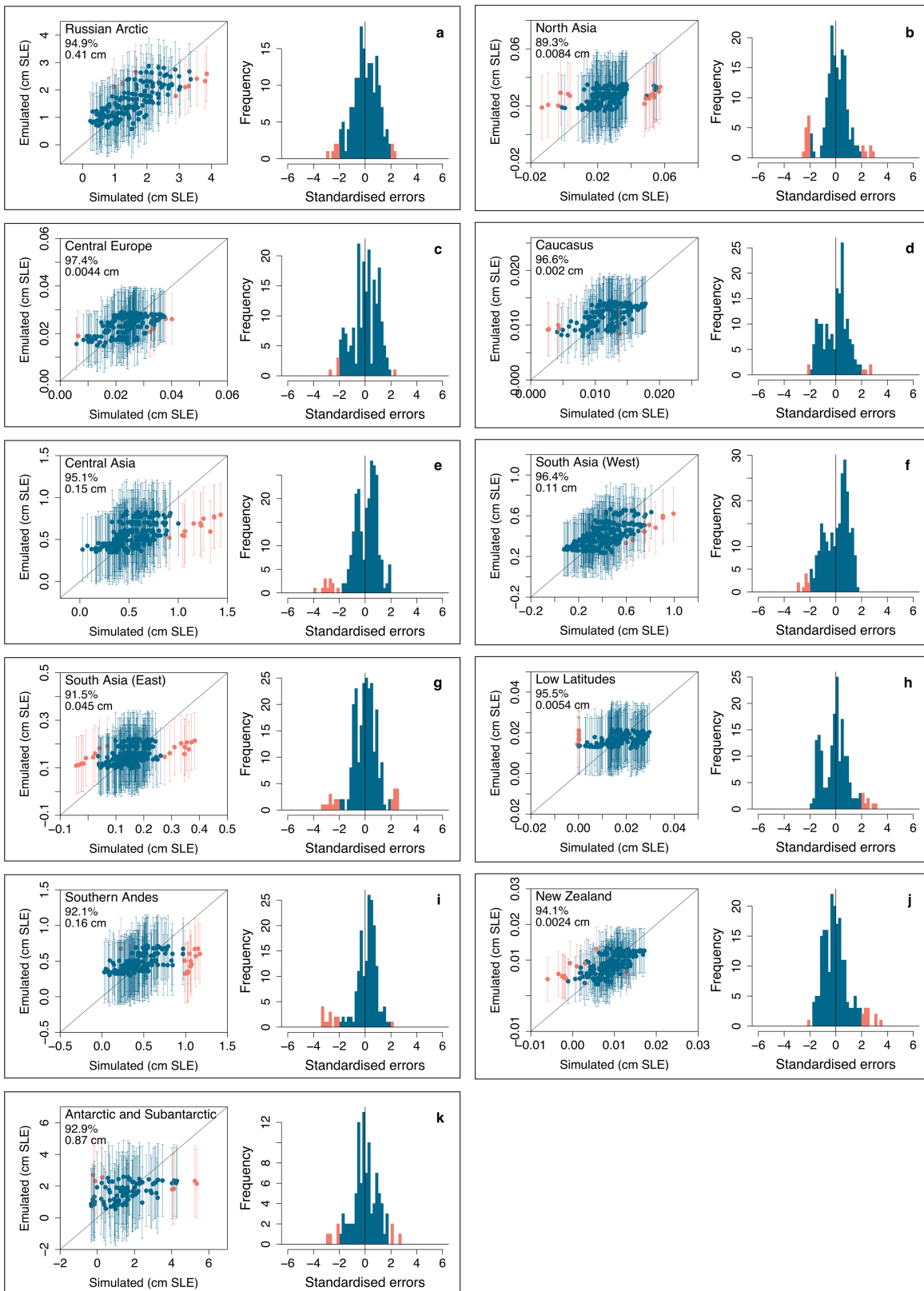
Reprints and permissions information is available at <http://www.nature.com/reprints>.



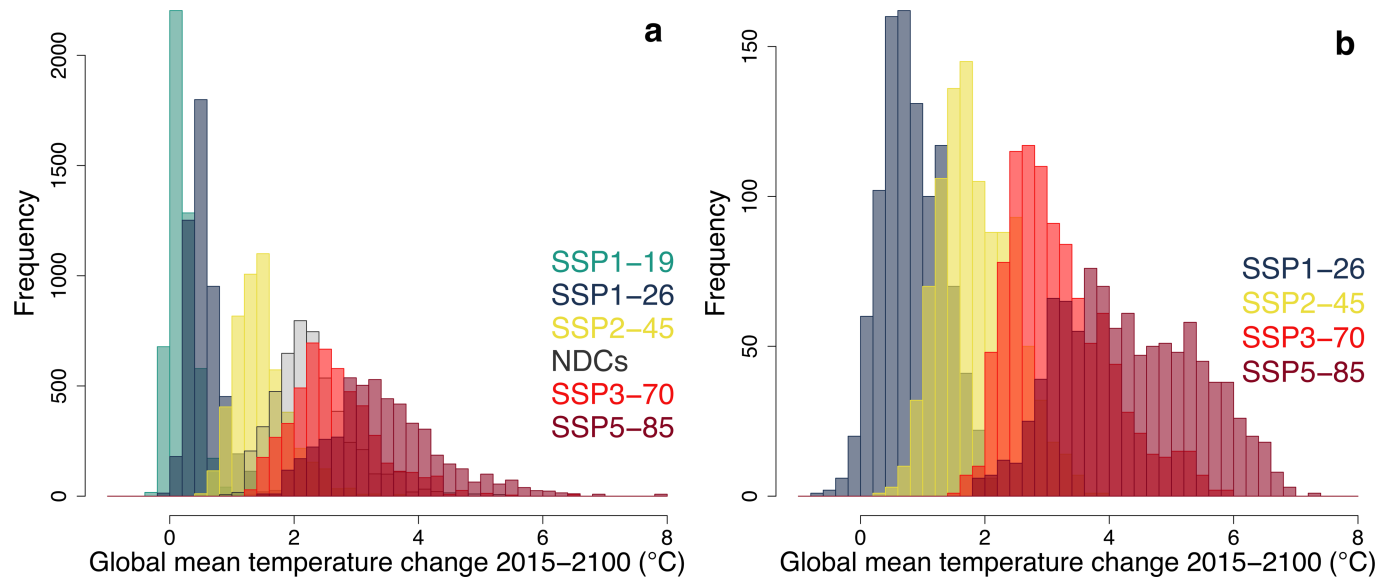
Extended Data Fig. 1 | Emulator leave-one-out validation for ice sheets and eight glacier regions. **a–l**, Left: emulator predictions versus simulations for each regional sea level contribution in the year 2100, with percentage of predictions falling outside ± 2 emulator standard deviations and mean absolute

error in cm SLE. Right: standardized residuals (emulated minus simulated, divided by emulator standard deviation). Predictions falling outside ± 2 emulator standard deviations are shown in orange.

Article

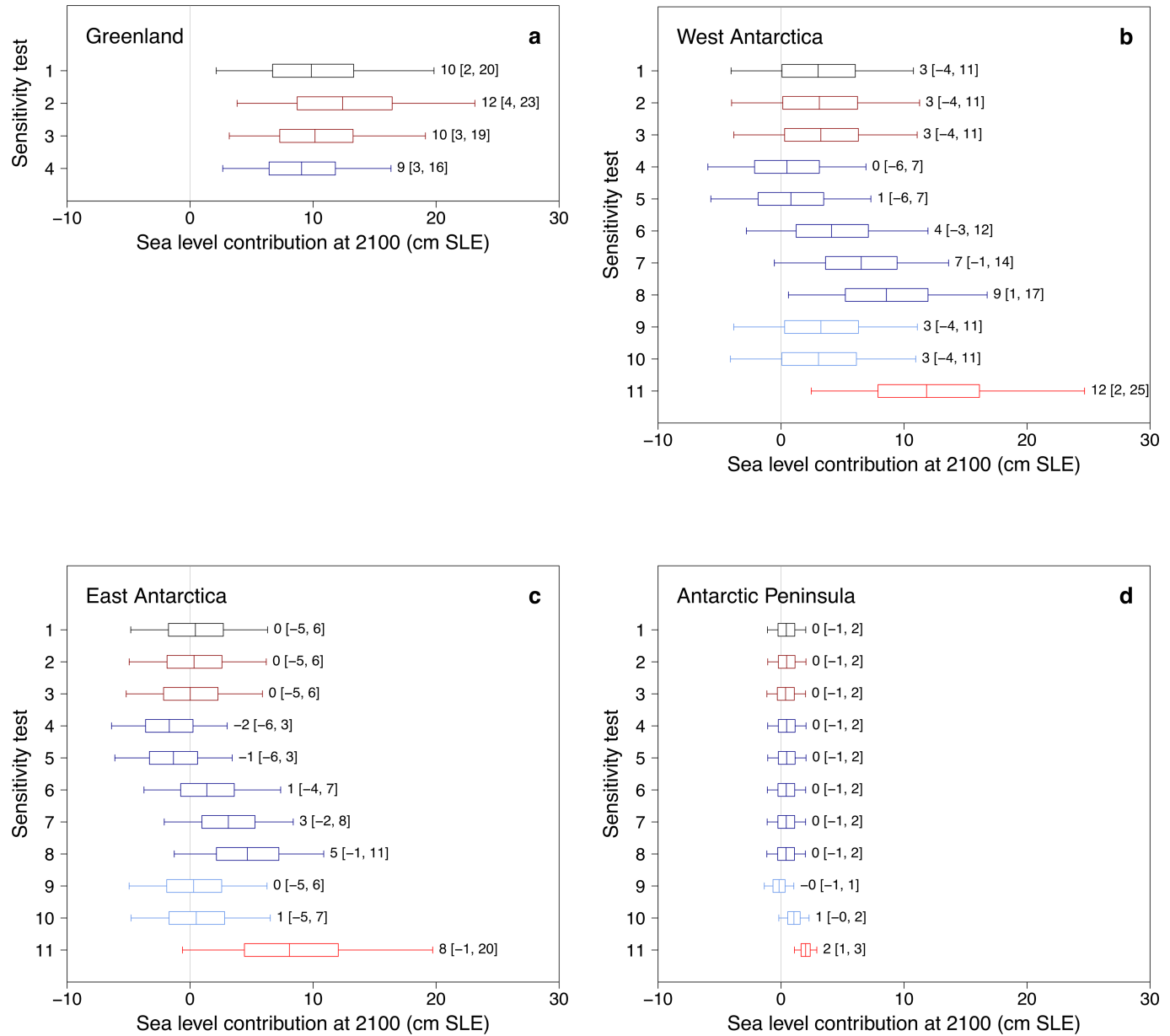


Extended Data Fig. 2 | Emulator leave-one-out validation for 11 glacier regions. As for Extended Data Fig. 1, but for the remaining glacier emulators.



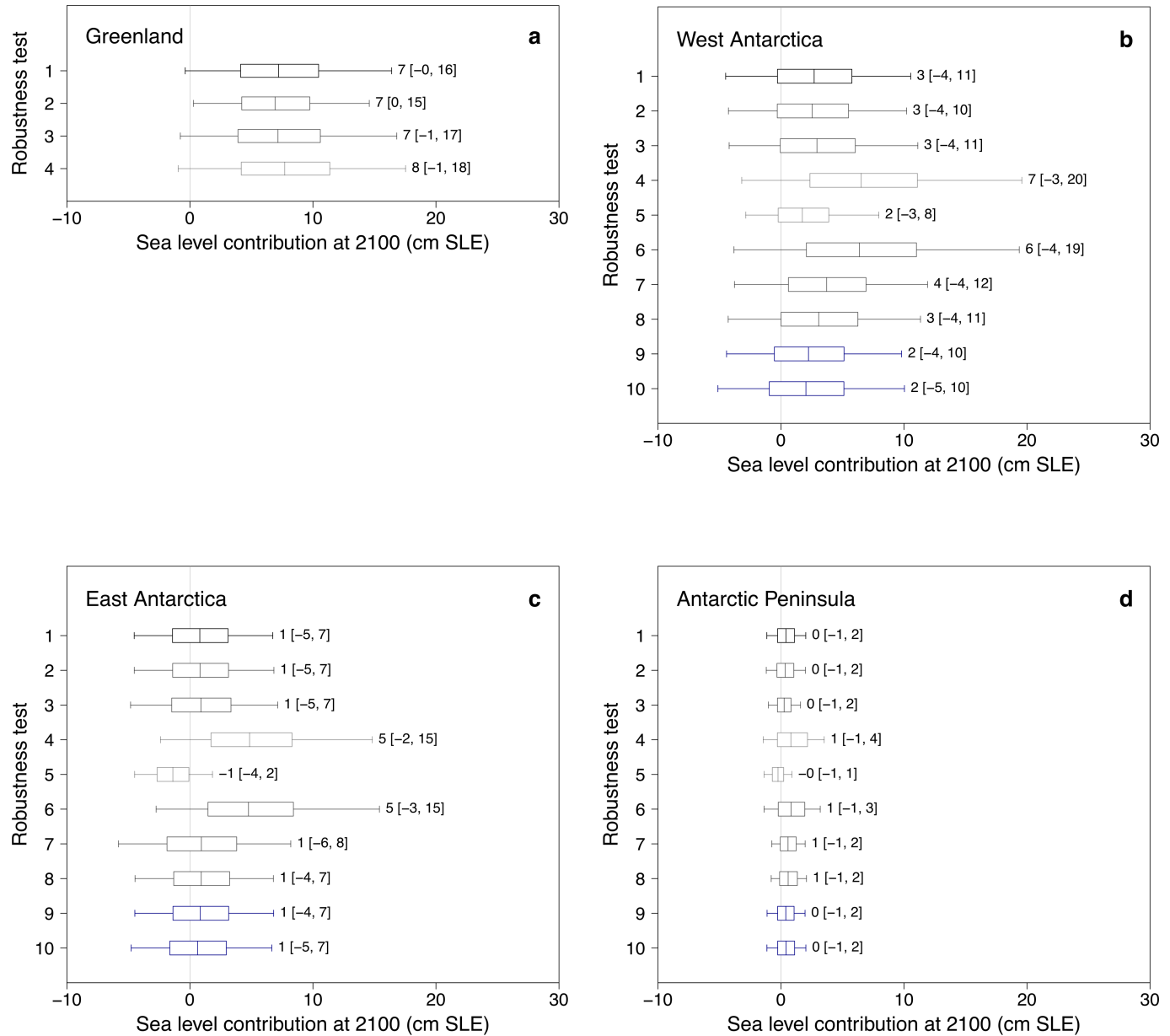
Extended Data Fig. 3 | Temperature projections for 2015–2100 from FaiR and CMIP6 ensembles. **a, b,** Global surface air temperature projections under different greenhouse gas scenarios (see text) from the FaiR simple climate

model ensemble (**a**; $N=5,000$; same as Fig. 3a), and CMIP6 global climate model ensemble (**b**; $N\approx 30$ models per scenario; see Methods) sampled with a kernel density estimate ($N=1,000$).



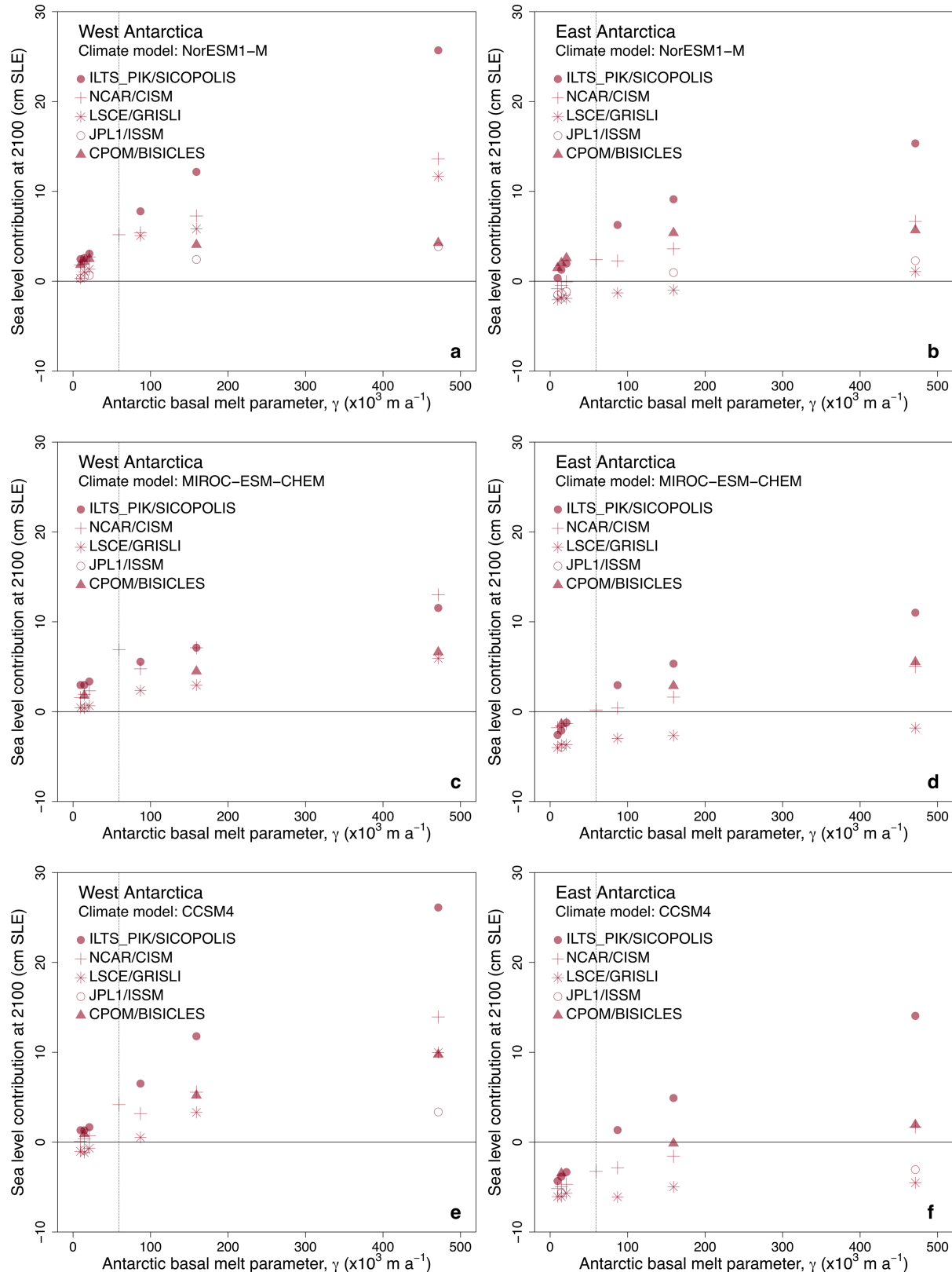
Extended Data Fig. 4 | Sensitivity of ice sheet projections at 2100 under SSP5-85 to uncertain inputs. **a**, Greenland. **b**, West Antarctica. **c**, East Antarctica. **d**, Antarctic Peninsula. Box and whiskers show [5, 25, 50, 75, 95]th percentiles. Indices refer to test (see Extended Data Table 3). Sensitivity test 1, default; 2, CMIP6 global climate model ensemble projections of global mean surface air temperature, instead of FaIR simple climate model; 3, fixed global mean surface air temperature; 4, fixed glacier retreat (Greenland) or basal melt

(Antarctica) parameter. Antarctic regions only: basal melt parameter has sensitivity test 5: ‘mean Antarctic’ distribution; 6, ‘Pine Island Glacier’ distribution; 7, uniform, high distribution; 8, uniform, very high distribution. Ice shelf collapse scenario: sensitivity test 9, off; 10, on. 11, Risk-averse projections using the high ‘Pine Island Glacier’ distribution for basal melt (test 6), ice shelf collapse on (test 10), and the ice sheet and climate models that give the highest sea level contributions (Extended Data Fig. 5; test 6, 7).



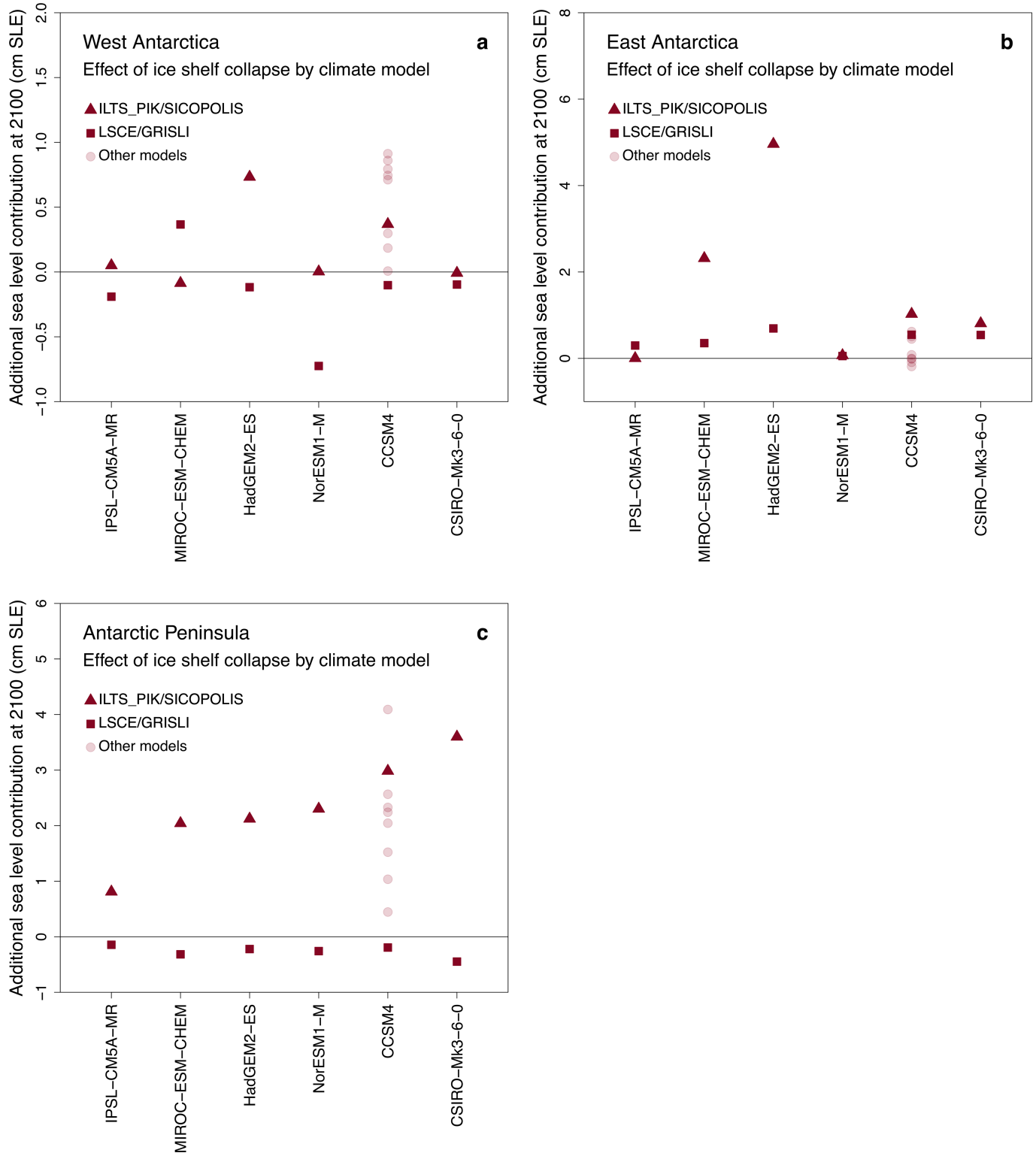
Extended Data Fig. 5 | Robustness of ice sheet projections under NDCs to ice sheet/climate model simulation selection and treatment. **a**, Greenland. **b**, West Antarctica. **c**, East Antarctica. **d**, Antarctic Peninsula. Box and whiskers show [5, 25, 50, 75, 95]th percentiles. Indices refer to test (see Extended Data Table 4). Robustness test 1, default; 2, higher-resolution ice sheet models; 3, ice sheet models with the most complete sampling of uncertainties (10 models for Greenland, four for Antarctica); 4, single ice sheet model with the most complete sampling of uncertainties and (coincidentally) high sensitivity to

retreat or basal melting parameter. Antarctic regions only: robustness test 5, alternative single ice sheet model with nearly as complete sampling but low sensitivity to basal melt parameter; 6, ice sheet models with the highest sensitivity to basal melt parameter; 7, climate models that lead to highest sea level contributions. 8, ice sheet models with 2015–2020 mass change in the range 0–0.6 cm SLE; 9, only ice sheet models that use the standard ISMIP melt parameterizations; 10, higher basal melt value assigned to ice sheet models that do not use the standard ISMIP6 melt parameterizations.



Extended Data Fig. 6 | Sensitivity to basal melting by Antarctic ice sheet and climate model. Vertical lines show ice sheet models that do not use the ISMIP6 basal melt parameterization, and the basal melt value they are assigned.

Ice sheet models include the high and low sensitivity models in Extended Data Fig. 5: test 4 (ILTS_PIK/SICOPOLIS) and test 5 (LSCE/GRISLI).



Extended Data Fig. 7 | Effect of Antarctic ice shelf collapse by climate model. Additional sea level contribution at 2100 when using ice shelf collapse for six climate models, ordered by maximum impact on the Peninsula contribution. **a**, West Antarctica; **b**, East Antarctica; and **c**, Antarctic Peninsula.

Article

Extended Data Table 1 | The additional 22 Greenland and 37 Antarctic ice sheet model experiments not previously described elsewhere

Additional Greenland experiments				
Experiment name	Scenario	Climate model	Retreat parameter	
expe01	RCP8.5	NorESM1-M	K ₉₅	
expe02	RCP8.5	NorESM1-M	K ₅	
expe03	RCP8.5	HadGEM2-ES	K ₉₅	
expe04	RCP8.5	HadGEM2-ES	K ₅	
expe05	RCP2.6	MIROC5	K ₉₅	
expe06	RCP2.6	MIROC5	K ₅	
expe07	RCP8.5	IPSL-CM5A-MR	K ₉₅	
expe08	RCP8.5	IPSL-CM5A-MR	K ₅	
expe09	RCP8.5	CSIRO-Mk3-6-0	K ₉₅	
expe10	RCP8.5	CSIRO-Mk3-6-0	K ₅	
expe11	RCP8.5	ACCESS1-3	K ₉₅	
expe12	RCP8.5	ACCESS1-3	K ₅	
expe13	SSP5-85	CNRM-CM6-1	K ₉₅	
expe14	SSP5-85	CNRM-CM6-1	K ₅	
expe15	SSP1-26	CNRM-CM6-1	K ₉₅	
expe16	SSP1-26	CNRM-CM6-1	K ₅	
expe17	SSP5-85	UKESM1-0-LL	K ₉₅	
expe18	SSP5-85	UKESM1-0-LL	K ₅	
expe21	SSP5-85	CNRM-ESM2-1	K ₉₅	
expe22	SSP5-85	CNRM-ESM2-1	K ₅	
expe23	RCP8.5	MIROC5	K ₉₅	
expe24	RCP8.5	MIROC5	K ₅	
Additional Antarctic experiments				
Experiment name	Scenario	Climate model	Basal melt (γ_0)	Ice shelf collapse (C)
Basal melt parameter values				
expD1	RCP8.5	MIROC-ESM-CHEM	MeanAnt ₉₅	Off
expD2	RCP8.5	MIROC-ESM-CHEM	MeanAnt ₅	Off
expD3	RCP2.6	NorESM1-M	MeanAnt ₉₅	Off
expD4	RCP2.6	NorESM1-M	MeanAnt ₅	Off
expD5	RCP8.5	CCSM4	MeanAnt ₉₅	Off
expD6	RCP8.5	CCSM4	MeanAnt ₅	Off
expD7	RCP8.5	HadGEM2-ES	MeanAnt ₉₅	Off
expD8	RCP8.5	HadGEM2-ES	MeanAnt ₅	Off
expD9	RCP8.5	CSIRO-Mk3-6-0	MeanAnt ₉₅	Off
expD10	RCP8.5	CSIRO-Mk3-6-0	MeanAnt ₅	Off
expD11	RCP8.5	IPSL-CM5A-MR	MeanAnt ₉₅	Off
expD12	RCP8.5	IPSL-CM5A-MR	MeanAnt ₅	Off
expD13	SSP5-85	CNRM-CM6-1	MeanAnt ₉₅	Off
expD14	SSP5-85	CNRM-CM6-1	MeanAnt ₅	Off
expD15	SSP5-85	UKESM1-0-LL	MeanAnt ₉₅	Off
expD16	SSP5-85	UKESM1-0-LL	MeanAnt ₅	Off
expD17	SSP5-85	CESM2	MeanAnt ₉₅	Off
expD18	SSP5-85	CESM2	MeanAnt ₅	Off
expD51	RCP8.5	NorESM1-M	PIG ₅	Off
expD52	RCP8.5	NorESM1-M	PIG ₉₅	Off
expD53	RCP8.5	MIROC-ESM-CHEM	PIG ₅₀	Off
expD54	RCP8.5	MIROC-ESM-CHEM	PIG ₅	Off
expD55	RCP8.5	MIROC-ESM-CHEM	PIG ₉₅	Off
expD56	RCP8.5	CCSM4	PIG ₅₀	Off
expD57	RCP8.5	CCSM4	PIG ₅	Off
expD58	RCP8.5	CCSM4	PIG ₉₅	Off
expT071	RCP2.6	NorESM1-M	PIG ₅₀	Off
expT072	RCP2.6	NorESM1-M	PIG ₅	Off
expT073	RCP2.6	NorESM1-M	PIG ₉₅	Off
Ice shelf collapse under different climate forcings				
expE6	RCP8.5	NorESM1-M	MeanAnt ₅₀	On
expE7	RCP8.5	MIROC-ESM-CHEM	MeanAnt ₅₀	On
expE8	RCP8.5	HadGEM2-ES	MeanAnt ₅₀	On
expE9	RCP8.5	CSIRO-Mk3-6-0	MeanAnt ₅₀	On
expE10	RCP8.5	IPSL-CM5A-MR	MeanAnt ₅₀	On
Ice shelf collapse and basal melt interactions				
expTD5	RCP8.5	CCSM4	MeanAnt ₉₅	On
expTD56	RCP8.5	CCSM4	PIG ₅₀	On
expTD58	RCP8.5	CCSM4	PIG ₉₅	On

Retreat parameter values κ_5 and κ_{95} are the 5th and 95th percentile values of the retreat (κ) distribution; basal melt parameter values MeanAnt_{5,50,95} and PIG_{5,50,95} are the 5th, 50th and 95th percentile values of the mean Antarctic and Pine Island Glacier basal melt (γ) distributions (see Methods).

Extended Data Table 2 | Emulator structure and validation

Region	Covariance function and hyperparameters (α : exponent; v : roughness parameter)	% predictions within emulator 95% interval	Mean absolute error (cm)
Greenland ice sheet	power exp ($\alpha = 0.1$)	94.1	1.4
West Antarctica	power exp ($\alpha = 0.1$)	93.6	2.0
East Antarctica	power exp ($\alpha = 0.1$)	94.8	1.5
Antarctic Peninsula	power exp ($\alpha = 0.1$)	92.4	0.28
1: Alaska	power exp ($\alpha = 1.0$)	95.5	0.55
2: Western Canada and U.S.	power exp ($\alpha = 1.9$)	96.1	0.040
3: Arctic Canada North	power exp ($\alpha = 1.9$)	92.7	0.51
4: Arctic Canada South	power exp ($\alpha = 0.1$)	95.5	0.27
5: Greenland periphery	power exp ($\alpha = 0.1$)	94.9	0.36
6: Iceland	power exp ($\alpha = 1.0$)	95.5	0.13
7: Svalbard	power exp ($\alpha = 0.1$)	95.5	0.37
8: Scandinavia	power exp ($\alpha = 1.0$)	98.3	0.012
9: Russian Arctic	power exp ($\alpha = 1.0$)	94.9	0.41
10: North Asia	power exp ($\alpha = 1.0$)	89.3	0.0084
11: Central Europe	power exp ($\alpha = 1.0$)	97.4	0.0044
12: Caucasus	Matérn ($v = 3/2$)	96.6	0.0020
13: Central Asia	power exp ($\alpha = 0.1$)	95.1	0.15
14: South Asia (West)	power exp ($\alpha = 1.9$)	96.4	0.11
15: South Asia (East)	power exp ($\alpha = 0.1$)	91.5	0.045
16: Low Latitudes	power exp ($\alpha = 0.1$)	95.5	0.0054
17: Southern Andes	Matérn ($v = 5/2$)	92.1	0.16
18: New Zealand	power exp ($\alpha = 0.1$)	94.1	0.0024
19: Antarctic and Subantarctic periphery	Matérn ($v = 5/2$)	92.9	0.87

Emulator covariance functions, and the results of the leave-one-out procedure for each: the percentage of simulations that fall within the emulator 95% uncertainty intervals, and the mean absolute error.

Article

Extended Data Table 3 | Sensitivity tests

Sensitivity tests	
Description	Impact
2: CMIP6 temperature projections Around 30 CMIP6 models are available at the time of analysis for four SSPs (31 for SSP1-26, 30 for SSP2-45, 27 for SSP3-70 and 31 for SSP5-85). Simulations are obtained and processed in the same way as the subset used for the emulator calibration. We set missing 2100 values to that of 2099 (for CAMS-CSM1-0, and two additional models for SSP3-70). We smooth the temperature changes with a kernel density estimator and sample from this with replacement ($N = 1000$; Extended Data Figure 3).	We find a slight increase in projected sea level rise: median and 95 th percentile land ice contributions increase by 1.5 cm and 4-7 cm across scenarios SSP1-26 to SSP5-85. This is likely due to the greater number of simulations with high equilibrium climate sensitivity in CMIP6 than Fair (and a wider range than several recent past generations, 1.8-5.6°C) ³³ . The Fair ensemble is constructed to have a climate sensitivity distribution in line with latest understanding from multiple lines of evidence (5-95% range 2-5°C) ¹² .
3, 4: Fixed global mean temperature and ice sheet melt parameters We replace the input distributions with single values, to test the potential for reducing uncertainties with improved knowledge	Using the Fair ensemble mean for global temperature, the width of the 5-95% range for SSP5-85 reduces from 30 cm to 26 cm. Using default values of the Greenland retreat and Antarctic basal melt parameters ($\kappa = \kappa_{50}$; $\gamma = \text{MeanAnt}_{50}$), the 5-95% range decreases from 30 cm to 25 cm.
5, 6: Antarctic basal melt - Mean Antarctic and Pine Island Glacier distributions We use the Mean Antarctic (test 5), or Pine Island Glacier (test 6) distribution for basal melt γ , rather than the combined distribution, sampling from the original distributions with replacement.	Results are discussed in the main text.
7, 8: Antarctic basal melt - uniform distributions We use two uniform distributions to reproduce the sampling strategy of ref [27]. This is an emulation-type study based on a similar ensemble of climate and Antarctic ice sheet models to ISMIP6, which uses a uniform distribution for basal melt sensitivity consistent with values estimated for the Amundsen Sea region ³⁸ . If we add projections of dynamic change from ref. [27] to IPCC AR5 ²⁶ projections for surface mass balance (SMB), neglecting differences in time period, the median projections are ~11 and ~13 cm under RCP2.6 and RCP8.5, and the 95 th percentiles are ~35 and ~54 cm (using median SMB values in both).	We reach similar values only with extreme values of the basal melt parameter: we show here $\gamma \sim \text{unif}[\text{PIG}_{50}, \text{PIG}_{95}]$ and $\gamma \sim \text{unif}[\text{PIG}_{50}, 700000]$, where 700000 is 98.7th percentile of the Pine Island Glacier distribution, which give median projections of 10 cm and ~14 cm across all scenarios. The 95 th percentiles are roughly half those of the other study: ~19 cm and ~24 cm.
9, 10: Antarctic ice shelf collapse off and on We use only $C = 0$ or $C = 1$, rather than a random sample of the two.	Results are discussed in the main text.
11: Risk-averse Antarctic projections We use the five global climate models with highest sea level contribution or for which ice shelf collapse projections are available (Robustness test 7), the four Antarctic ice sheet models with highest sensitivity to basal melting (Robustness test 6), the Pine Island Glacier distribution for basal melt γ (Sensitivity test 6) and ice shelf collapse on (Sensitivity test 10). We also use the same γ value for all three regions in a given projection, i.e. fully correlated rather than sampled independently, to explore the tails more fully: this aspect broadens the distribution, increasing the 95 th percentile by 2-4 cm and decreasing the 5 th by 1 cm, and also decreases the median by 1 cm. We use $N = 5000$ temperature samples, as for the main projections. We do not use the combinations that lead to the highest possible sea level contribution – i.e. the single most sensitive ice sheet model (Robustness test 4), or the extreme distributions for basal melt (Sensitivity test 7-8) – because we aim to provide plausible high-end projections, rather than relying on a single model or unrealistic assumptions.	Results are discussed in the main text.

Tests of the sensitivity of the ice sheet projections to changes in the chosen inputs. The test index, name, description and impact are detailed. Numerical values refer to changes in the median and [5th, 95th] percentile estimates for the ice sheet under SSP5-85, unless otherwise stated; results for this scenario are shown in Extended Data Fig. 4. Refs. ^{12,26,27,33,38}. See also Supplementary Information.

Extended Data Table 4 | Robustness checks

Robustness checks	
Description	Impact
2: High resolution models We use only Greenland ice sheet models with minimum spatial resolution less than 8 km (N = 215) and Antarctic ice sheet models with resolution less than 32 km (N = 303).	This results in differences of 0-1 cm for each ice sheet.
3: More balanced design We restrict the input dataset to only the models with the most complete designs (i.e. the most experiments). For Greenland, we use 10 of the 21 models: one with 28 experiments (IMAU/IMAUICE1) and the nine models that ran all 14 experiments presented by refs. [6] and [8] (AWI/ISSM1, ISSM2 and ISSM3, ILTS_PIK/SICOPOLIS1 and SICOPOLIS2, JPL/ISSM, LSCE/GRISLI2, NCAR/CISM, VUB/GISMHOMv1), removing the dummy variable from the emulator as there are no 'open' models in this set (N = 154). For Antarctica, we use four of the 16 models (ILTS_PIK/SICOPOLIS: N = 55, of which 13 do not use the ISMIP6 parameterisation; JPL/ISSM: N = 48; LSCE/GRISLI: N = 47; NCAR/CISM: N = 27) (total N = 177).	This results in differences of 0-1 cm for each ice sheet.
4, 5: Single ice sheet models We use only the Greenland model with the most simulations (IMAU/IMAUICE1: N = 28), and a single model for Antarctica (test 4: ILTS_PIK/SICOPOLIS, N = 48; test 5: LSCE/GRISLI, N = 47). The two Antarctic models have high and low sensitivity to the basal melting parameter, respectively (Extended Data Figure 6).	Using one Greenland model has little impact: the largest change is 2 cm increase in the 95 th percentile, due to this model being at the upper end of the range in sensitivity to the retreat parameter (Figure 2a: triangles). Using one Antarctic model has far more effect: results are discussed further in the main text.
6: Highest sensitivity Antarctic ice sheet models We use the four Antarctic models with highest sensitivity to basal melting, i.e. largest 2100 contribution for $\gamma = \text{PIG}_{50}$, ice shelf collapse off and RCP8.5/SSP5-85 (decreasing order: ILTS_PIK/SICOPOLIS: N = 48; ULB/ETISH_16km: N = 21; ULB/ETISH_32km: N = 21; DOE/MALI: N = 8) (total N = 98).	Results are discussed in the main text.
7: Select climate models that result in highest Antarctic sea level contributions We use only results from the climate models that lead to highest sea level contributions at 2100 under $\gamma = \text{MeanAnt}_{50}$, ice shelf collapse off and RCP8.5/SSP5-85 (in decreasing order: HadGEM2-ES, UKESM1-0-LL, MIROC-ESM-CHEM, NorESM1-M). We also include CCSM4, to retain information on the effect of ice shelf collapse (N = 241). We also test the impact of using only two of these climate models (not shown in Extended Data Figure 5): NorESM1-M (discussed in the main text regarding scenario-dependence: Figure 4) and CCSM4 (for shelf collapse) (N = 164).	Using these five climate models results in +1 cm change to median from SSP1-19 to SSP5-85 for West Antarctica, -1 cm for East Antarctica, and +1 cm for the total. NDCs median increases by +2 cm relative to main projections. Using only NorESM1-M and CCSM4 leads to +2 cm from SSP1-19 to SSP5-85 for West Antarctica, -3 cm for East Antarctica, and -3 cm decrease for the total, i.e. a weak scenario dependence; no change to NDCs median.
8: Exclude Antarctic ice sheet models far from observed trend We exclude simulations with 2015-2020 sea level contributions outside the range 0.00-0.60 cm, motivated by recent observations. We use a satellite estimate ⁶⁵ of the mass trend from 2012-2017 ($-219 \pm 43 \text{ Gt a}^{-1}$) and reject simulations for which the mean trend over 2015-2020 is outside the mean ± 5 s.d. interval (N = 181). We choose this interval to allow for the trend changing from one time period to the other, and for tolerance to model discrepancy ²⁵ , and because it coincides with zero at the bottom end so is informative for excluding models with mass gain at the start of the projections (as well as those with very rapid mass loss).	This results in +1 cm scenario-dependence for West Antarctica and -2 cm for East Antarctica, and none for the total; the NDCs median increases by 1 cm.
9: Exclude Antarctic ice sheet models that do not use ISMIP6 melt parameterisation We exclude the ice sheet models that do not use the ISMIP6 basal melt parameterisation. (N = 282).	No scenario-dependence for West Antarctica or the total; -2 cm for East Antarctica. No change to NDCs median.
10: Impute higher basal melt value for Antarctic ice sheet models that do not use the ISMIP6 melt parameterisation We assign models that do not use the ISMIP6 parameterisations a higher value for γ (150,000; slightly less than PIG_{50}), rather than the ensemble mean (59,317), reflecting the fact that such models are often tuned to Amundsen Sea (high) melt observations, and approximately in line with NCAR/CISM which was run in both modes (Extended Data Figure 6).	This results in +1 cm scenario-dependence for West Antarctica, -1 cm decrease for East Antarctica, and no change for the total; the NDCs median projection decreases by 1 cm.

Checks performed to test the robustness of the ice sheet projections to changes in the simulation dataset. The test index, name, description and impact are detailed. Numerical values refer to changes in the median and [5, 95]th percentile estimates for the ice sheet under the NDCs scenario, unless otherwise stated; results for this scenario are shown in Extended Data Fig. 5. Refs. ^{6,8,25,65}. See also Supplementary Information.